Valence quark, sea, and gluon content of the pion from the parton distribution functions and the electromagnetic form factor

Barbara Pasquini,[1,2,*] Simone Rodini,[3,†] and Simone Venturini[1,2,‡]

(MAP Collaboration)[§]

[1]*Dipartimento di Fisica, Università degli Studi di Pavia, I-27100 Pavia, Italy*
[2]*Istituto Nazionale di Fisica Nucleare, Sezione di Pavia, I-27100 Pavia, Italy*
[3]*CPHT, CNRS, Ecole Polytechnique, Institut Polytechnique de Paris, Route de Saclay, 91128 Palaiseau, France*

(Received 10 March 2023; accepted 9 May 2023; published 15 June 2023)

We present a light-front model calculation of the pion parton distribution functions (PDFs) and the pion electromagnetic form factor. The pion state is modeled in terms of light-front wave functions (LFWFs) for the $q\bar{q}$, $q\bar{q}q\bar{q}$, $q\bar{q}g$, and $q\bar{q}gg$ components. We design the LFWFs so that the parameters in the longitudinal- and transverse-momentum space enter separately in the fit of the pion PDFs and the electromagnetic form factor, respectively. We extract the pion PDFs within the xFitter framework using available Drell-Yan and photon-production data. With the obtained parameters in the longitudinal-momentum space, we then fit the available experimental data on the pion electromagnetic form factor to constrain the remaining parameters in the transverse-momentum space. The results for the pion PDFs are compatible with existing extractions and lattice calculations, and the fit to the pion electromagnetic form factor data works quite successfully. The obtained parametrization for the LFWFs marks a step forward toward a unified description of different hadron distribution functions in both the longitudinal- and transverse-momentum space and will be further applied to a phenomenological study of transverse-momentum-dependent parton distribution functions and generalized parton distributions.

DOI: 10.1103/PhysRevD.107.114023

I. INTRODUCTION

A successful approach in high-energy scattering is based on light-front quantization where hadrons are described by light-front wave functions (LFWFs) [1]. The latter are expressed as an expansion of various quark (q), antiquark ($\bar{q}$), and gluon (g) Fock components. Schematically, a pion state is conceived as the following superposition:

$$|\pi\rangle = \psi_{q\bar{q}}|q\bar{q}\rangle + \psi_{q\bar{q}q\bar{q}}|q\bar{q}q\bar{q}\rangle + \psi_{q\bar{q}g}|qqg\rangle + \psi_{q\bar{q}gg}|q\bar{q}gg\rangle + \ldots, \quad (1)$$

where, in the light-cone gauge $A^+ = 0$, the LFWF ψ for each parton configuration involves a number of independent amplitudes corresponding to different combinations of quark orbital angular momentum and helicity [2]. The light-front representation has a number of simplifying properties. In particular, it allows one to describe the hadronic matrix elements which parametrize the soft contribution in inclusive and exclusive reactions in terms of overlap of LFWFs with different parton configurations [3]. A variety of phenomenological and theoretical models have been devised to give explicit expressions for the LFWF amplitudes and to access information on the internal structure of the pion from different partonic functions. In this work, we will restrict ourselves to investigating the pion parton distributions (PDFs) and pion electromagnetic (e.m.) form factor.

Most models for the pion PDFs confined the study to the valence quark distributions or included a dynamical gluon at the hadronic scale of the model with the sea quark contribution generated perturbatively by QCD evolution [4–28]. In the last few years, there has been also an increasing number of calculations of x-dependent pion PDFs in lattice QCD following different approaches. They have been mainly

*barbara.pasquini@unipv.it
†simone.rodini@polytechnique.edu
‡simone.venturini01@universitadipavia.it

§The MAP acronym stands for "Multi-dimensional Analyses of Partonic distributions." It refers to a collaboration aimed at studying the three-dimensional structure of hadrons.

Published by the American Physical Society under the terms of the Creative Commons Attribution 4.0 International license. Further distribution of this work must maintain attribution to the author(s) and the published article's title, journal citation, and DOI. Funded by SCOAP³.

restricted to the valence quark sector [29–37] and only recently have been extended to the gluon sector [38]. Complementing these theory developments, global analyses of pion PDFs have been performed mostly using pion-induced Drell-Yan (DY) data and J/ψ-production data or direct photon production [39–50]. However, the current knowledge of the pion PDFs is less accurate than for the nucleon PDFs, mainly because there are fewer experimental data to constrain the pion PDFs, especially for the sea quark and gluon contributions. New experiments are expected to further our knowledge of the pion PDFs. The planned experiments at Jefferson Lab (JLab) [51] and at new-generation facilities using high-luminosity electron-proton collisions [52,53] are developing the capacity to access the pion PDFs via the Sullivan process [54], consisting of scattering off the pion in proton to pion fluctuations [55,56]. Furthermore, experiments from COMPASS++/AMBER will exploit high-energy, high-intensity pion beams to probe directly the partonic structure of the pion [57].

Different insights into the pion structure can be gained from the study of the pion e.m. form factor. The e.m. form factor probes the charge distribution in the pion and is a good observable for studying the onset, with increasing energy, of the perturbative QCD regime for exclusive processes [58,59]. It has been successfully described in a variety of light-front quark models [4,6,9,21,22,60–67] and has witnessed enormous progress in recent lattice QCD calculations [68–82]. Data for the pion e.m. form factor at low momentum transfer ($Q^2 \leq 0.253$ GeV^2) have been measured at Fermilab [83,84] and CERN [85,86] by scattering of pions off atomic electrons and were used to extract also the pion charge radius. At higher momentum transfer, up to $Q^2 \approx 10$ GeV^2, the pion e.m. form factor was extracted in experiments of pion electroproduction in Cornell [87–89], DESY [90,91], and JLab [92–96], by exploiting the Sullivan mechanism. New accurate data are expected at intermediate values of Q^2 from upcoming JLab measurements [51] while the future electron-ion colliders will potentially give access to the region at higher momentum transfer, up to $Q^2 = 30$ GeV^2.

In this work, we propose a new parametrization of the pion LFWFs which comprises the Fock states of the $q\bar{q}$, $q\bar{q}q\bar{q}$, $q\bar{q}g$, and $q\bar{q}gg$ components and is adapted to reproduce simultaneously the available experimental data on the pion PDFs and e.m. form factor. To our knowledge, the expansion in the Fock space up to the two-gluon component represents the largest basis that has been used so far in light-front model calculations of the pion PDFs and e.m. form factor. Furthermore, we design the LFWFs so that the parameters in the longitudinal- and transverse-momentum space enter separately in the fit of the pion PDFs and e.m. form factor, respectively. In particular, the parametrization in the longitudinal-momentum space is dictated by the pion distribution amplitudes, while the functional form in the transverse-momentum space is constrained so that the LFWF overlap representation of the pion PDFs does not depend on the transverse-momentum-dependent parameters. The fit to the experimental data of the pion PDF is performed using the open-source tool xFitter [97] which was recently extended to extract the pion PDF [98]. With the obtained parameters in the longitudinal-momentum space, we then fit the available experimental data on the pion e.m. form factor to constrain the parameters in the transverse-momentum space. Our results for the valence, sea, and gluon contribution to the pion PDFs are consistent with recent extractions [44,48,98], although the considered set of experimental data does not constrain well the sea and gluon contributions. Furthermore, the fit to the available experimental data for the pion e.m. form factor works very successfully, proving the merit of the adopted strategy to build the parametrization of the LFWFs.

The paper is organized as follows. After a brief review of the light-front Fock-space expansion of the pion state in Sec. II, we construct the explicit parametrization for the LFWFs in Sec. III. The pion PDFs are discussed in Sec. IV, where we present the model expressions of the pion PDFs obtained through the LFWF overlap representation. We then summarize the fit procedure of the pion PDFs within the xFitter framework and discuss the results in comparison with other recent extractions and model calculations. Section V is dedicated to the pion e.m. form factor, discussing the results from the fit to extant experimental data. In Sec. VI we summarize our results and give an outlook. Technical details about the LFWF overlap representation of the pion PDF and e.m. form factor are given in Appendixes A and B, respectively.

II. LIGHT-FRONT WAVE AMPLITUDES

In this section, we review the classification of the light-front wave functions of the pion, considering the Fock-space configuration up to four partons, i.e.,

$$|\pi(P)\rangle = |\pi(P)\rangle_{q\bar{q}} + |\pi(P)\rangle_{q\bar{q}g} + |\pi(P)\rangle_{q\bar{q}gg} + \sum_{\{\jmath\bar{\jmath}\}} |\pi(P)\rangle_{q\bar{q}\{\jmath\bar{\jmath}\}}, \tag{2}$$

where $q = u, d$ and the sum in $\{\bar{\jmath}\jmath\}$ runs over the N_f-flavor pairs of the sea quarks ($u\bar{u}$, $d\bar{d}$, $s\bar{s}$ at the model scale). The LFWF for each parton configuration can be classified according to the total parton light-cone helicity λ or, equivalently, to the angular momentum projection $l_z = -\lambda$, which follows from angular momentum conservation [2]. In principle, the states up to four partons in Eq. (2) involve 94 independent light-front wave amplitudes (LFWAs), corresponding to all the possible combinations of parton helicities. In order to keep the model as simple as possible, in our analysis we restrict ourselves to consider only the projection on the $l_z = 0$ component, i.e.,

$$|\pi(P)\rangle^{l_z=0} = |\pi(P)\rangle^{l_z=0}_{q\bar{q}} + |\pi(P)\rangle^{l_z=0}_{q\bar{q}g} + |\pi(P)\rangle^{l_z=0}_{q\bar{q}gg} + \sum_{\{\mathcal{J}\bar{\mathcal{J}}\}} |\pi(P)\rangle^{l_z=0}_{q\bar{q}\{\mathcal{J}\bar{\mathcal{J}}\}}. \tag{3}$$

Compared to the original classification in Ref. [2], we make the further simplification of neglecting the LFWAs that are multiplied by coefficients depending on the parton transverse momenta, in order to have simpler relations to the pion distribution amplitudes, as discussed in Sec. III. We then have the following expressions:

$$|\pi(P)\rangle^{l_z=0}_{q\bar{q}} = \int d[1]d[2] \frac{\delta_{c_1c_2}}{\sqrt{3}} \psi^{(1)}_{q\bar{q}}(1,2)[q^\dagger_{c_1\uparrow}(1)\bar{q}^\dagger_{c_2\downarrow}(2) - q^\dagger_{c_1\downarrow}(1)\bar{q}^\dagger_{c_2\uparrow}(2)]|0\rangle, \tag{4}$$

$$|\pi(P)\rangle^{l_z=0}_{q\bar{q}g} = \int d[1]d[2]d[3] \frac{T^a_{c_1c_2}}{2} \psi^{(1)}_{q\bar{q}g}(1,2,3)[(q\bar{q})^\dagger_{A,1} g^\dagger_{a\downarrow}(3) - (q\bar{q})^\dagger_{A,-1} g^\dagger_{a\uparrow}(3)]|0\rangle, \tag{5}$$

$$|\pi(P)\rangle^{l_z=0}_{q\bar{q}gg} = \int d[1]d[2]d[3]d[4] \frac{\delta_{c_1c_2}\delta^{ab}}{\sqrt{24}} \{\psi^{(1)}_{q\bar{q}gg}(1,2,3,4)(q\bar{q})^\dagger_{A,0}(gg)^\dagger_{S,0} + \psi^{(2)}_{q\bar{q}gg}(1,2,3,4)(q\bar{q})^\dagger_{S,0}(gg)^\dagger_{A,0}\}|0\rangle, \tag{6}$$

$$\begin{aligned}|\pi(P)\rangle^{l_z=0}_{q\bar{q}\{\mathcal{J}\bar{\mathcal{J}}\}} = \int d[1]d[2]d[3]d[4] \frac{\delta_{c_1c_2}\delta_{c_3c_4}}{3} &\{\psi^{(1)}_{q\bar{q}\mathcal{J}\bar{\mathcal{J}}}(1,2,3,4)(q\bar{q})^\dagger_{A,0}(\mathcal{J}\bar{\mathcal{J}})^\dagger_{S,0} + \psi^{(2)}_{q\bar{q}\mathcal{J}\bar{\mathcal{J}}}(1,2,3,4)(q\bar{q})^\dagger_{S,0}(\mathcal{J}\bar{\mathcal{J}})^\dagger_{A,0} \\ &+ \psi^{(3)}_{q\bar{q}\mathcal{J}\bar{\mathcal{J}}}(1,2,3,4)[(q\bar{q})^\dagger_{A,1}(\mathcal{J}\bar{\mathcal{J}})^\dagger_{A,-1} - (q\bar{q})^\dagger_{A,-1}(\mathcal{J}\bar{\mathcal{J}})^\dagger_{A,1}]\}|0\rangle,\end{aligned} \tag{7}$$

where $q^\dagger_{c\lambda}$ and $\bar{q}^\dagger_{c\lambda}$ are creation operators of a quark and antiquark with flavor q, helicity λ, and color c, respectively. The LFWAs ψ are functions of parton momenta with arguments $i = (x_i, \boldsymbol{k}_{\perp i})$ representing the fraction of longitudinal parton momentum $x_i = k^+_i/P^+$ and the transverse parton momentum $\boldsymbol{k}_{\perp i}$. Furthermore, in Eqs. (4)–(7), $T^a_{ij} = \frac{\lambda^a_{ij}}{2}$ are the SU(3) color matrices and the following operators have been introduced:

$$(q\bar{q})^\dagger_{S,0} = q^\dagger_{c_1\uparrow}(1)\bar{q}^\dagger_{c_2\downarrow}(2) + q^\dagger_{c_1\downarrow}(1)\bar{q}^\dagger_{c_2\uparrow}(2), \qquad (\mathcal{J}\bar{\mathcal{J}})^\dagger_{S,0} = \mathcal{J}^\dagger_{c_3\uparrow}(3)\bar{\mathcal{J}}^\dagger_{c_4\downarrow}(4) + \mathcal{J}^\dagger_{c_3\downarrow}(3)\bar{\mathcal{J}}^\dagger_{c_4\uparrow}(4), \tag{8}$$

$$(q\bar{q})^\dagger_{A,0} = q^\dagger_{c_1\uparrow}(1)\bar{q}^\dagger_{c_2\downarrow}(2) - q^\dagger_{c_1\downarrow}(1)\bar{q}^\dagger_{c_2\uparrow}(2), \qquad (\mathcal{J}\bar{\mathcal{J}})^\dagger_{A,0} = \mathcal{J}^\dagger_{c_3\uparrow}(3)\bar{\mathcal{J}}^\dagger_{c_4\downarrow}(4) - \mathcal{J}^\dagger_{c_3\downarrow}(3)\bar{\mathcal{J}}^\dagger_{c_4\uparrow}(4), \tag{9}$$

$$(q\bar{q})^\dagger_{A,1} = q^\dagger_{\uparrow c_1}(1)\bar{q}^\dagger_{c_2\uparrow}(2), \qquad (\mathcal{J}\bar{\mathcal{J}})^\dagger_{A,1} = \mathcal{J}^\dagger_{\uparrow c_3}(3)\bar{\mathcal{J}}^\dagger_{c_4\uparrow}(4), \tag{10}$$

$$(q\bar{q})^\dagger_{A,-1} = q^\dagger_{\downarrow c_1}(1)\bar{q}^\dagger_{c_2\downarrow}(2), \qquad (\mathcal{J}\bar{\mathcal{J}})^\dagger_{A,-1} = \mathcal{J}^\dagger_{\downarrow c_3}(3)\bar{\mathcal{J}}^\dagger_{c_4\downarrow}(4), \tag{11}$$

$$(gg)^\dagger_{S,0} = g^\dagger_{a\uparrow}(3)g^\dagger_{b\downarrow}(4) + g^\dagger_{a\downarrow}(3)g^\dagger_{b\uparrow}(4), \tag{12}$$

$$(gg)^\dagger_{A,0} = g^\dagger_{a\uparrow}(3)g^\dagger_{b\downarrow}(4) - g^\dagger_{a\downarrow}(3)g^\dagger_{b\uparrow}(4). \tag{13}$$

The integration measure in Eqs. (4)–(7) is defined as

$$\prod_{i=1}^N d[i] = [dx]_N [d^2\boldsymbol{k}_\perp]_N, \tag{14}$$

where

$$[dx]_N = \prod_{i=1}^N \frac{dx_i}{\sqrt{x_i}} \delta\left(1 - \sum_{i=1}^N x_i\right), \qquad [d^2\boldsymbol{k}_\perp]_N = \frac{1}{[2(2\pi)^3]^{N-1}} \prod_{i=1}^N d^2\boldsymbol{k}_{\perp i} \delta^{(2)}\left(\sum_{i=1}^N \boldsymbol{k}_{\perp i}\right). \tag{15}$$

III. MODEL FOR THE LFWAS

In order to construct a model with a realistic structure for the LFWAs, we will exploit their connection to the pion distribution amplitudes (DAs), which are pion-to-vacuum transition matrix elements of collinear operators [99–103]. Without loss of generality, we can write any LFWA as

$$\psi^{(i)}(1,2,\ldots,N) = \phi^{(i)}(x_1,x_2,\ldots,x_N)\Omega^{(i)}_{N,\beta}(x_1,\boldsymbol{k}_{\perp 1},x_2,\boldsymbol{k}_{\perp 2},\ldots,x_N,\boldsymbol{k}_{\perp N}), \tag{16}$$

where we introduced the label β for the parton composition $\{q\bar{q}, q\bar{q}g, q\bar{q}\jmath\bar{\jmath}, q\bar{q}gg\}$.

The integral over the intrinsic transverse momenta of the LFWA for $l_z = 0$ state with N partons can be expressed as a linear combination of DAs of N partons of matching type. Schematically,

$$\int [d^2\boldsymbol{k}_\perp]_N \psi^{(i)}(1,2,\ldots,N) = \sum_j a_{ij} d_j(x_1,\ldots,x_N), \tag{17}$$

where $d_j(x_1,\ldots,x_N)$ are the DAs. This relation is valid at the level of the bare operators. If one assumes that the $\Omega^{(i)}_{N,\beta}$ functions are normalized to unity, i.e.,

$$\int [d^2\boldsymbol{k}_\perp]_N \psi^{(i)}(1,2,\ldots,N) = \phi^{(i)}_N(x_1,\ldots,x_N) \int [d^2\boldsymbol{k}_\perp]_N \Omega^{(i)}_{N,\beta}(x_1,\boldsymbol{k}_{\perp 1},x_2,\boldsymbol{k}_{\perp 2},\ldots,x_N,\boldsymbol{k}_{\perp N}) = \phi^{(i)}_N(x_1,\ldots,x_N), \tag{18}$$

then we have the identification $\phi^{(i)}_N = \sum_j a_{ij} d_j$. Notice that we can always impose that normalization to the $\Omega^{(i)}_{N,\beta}$ functions if we do not assume specific boundary conditions for the ϕ functions. In fact, given Eq. (17), we can always introduce $\phi^{(i)}_N = \sum_j a_{ij} d_j$ and decompose

$$\psi^{(i)}_N = \phi^{(i)}_N(x_1,\ldots,x_N)\left(\frac{\psi^{(i)}_N(x_1,\boldsymbol{k}_{\perp 1},\ldots,x_N,\boldsymbol{k}_{\perp N})}{\phi^{(i)}_N(x_1,\ldots,x_N)}\right), \tag{19}$$

where the function in brackets can be named $\Omega^{(i)}_{N,\beta}$ and obviously satisfies the normalization condition

$$\int [d^2\boldsymbol{k}_\perp]_N \Omega^{(i)}_{N,\beta} = 1. \tag{20}$$

In the explicit construction of the LFWAs, we make a few assumptions. First, we take the same $\Omega^{(i)}_{N,\beta}$ function for each N-parton state, independent of the different helicity structure of the N partons. Specifically, we impose

$$\Omega^{(1)}_{4,q\bar{q}gg} = \Omega^{(2)}_{4,q\bar{q}gg}, \qquad \Omega^{(1)}_{4,q\bar{q}\jmath\bar{\jmath}} = \Omega^{(2)}_{4,q\bar{q}\jmath\bar{\jmath}} = \Omega^{(3)}_{4,q\bar{q}\jmath\bar{\jmath}}. \tag{21}$$

This assumption is motivated by the fact that the different $\Omega^{(i)}_{N,\beta}$ functions for a given N,β Fock state contribute to the PDF only through the normalization factor in Eq. (25b) that is independent of the different partons' configuration. We also verified that the fit to the available experimental data for the form factor is not able to distinguish between different functional forms for the $\Omega^{(i)}_{N,\beta}$ of a given N,β Fock state. Accordingly, hereafter we can omit the label (i) in the $\Omega^{(i)}_{N,\beta}$ functions. Moreover, we adopt an analogous simplification for the longitudinal-momentum dependence, as discussed in Sec. IV.

A. Model for the transverse-momentum dependence

For the functions $\Omega_{N,\beta}$ in Eq. (16), we adopt the Brodsky-Huang-Lepage [104] prescription which gives

$$\Omega_{N,\beta}(x_1,\boldsymbol{k}_{\perp 1},x_2,\boldsymbol{k}_{\perp 2},\ldots,x_N,\boldsymbol{k}_{\perp N}) = \frac{(16\pi^2 a_\beta^2)^{N-1}}{\prod_{i=1}^N x_i}\exp\left(-a_\beta^2\sum_{i=1}^N \frac{\boldsymbol{k}^2_{\perp i}}{x_i}\right). \tag{22}$$

The function in Eq. (22) satisfies the normalization condition in Eq. (20) and the following integral relation:

$$\int [d^2\boldsymbol{k}_\perp]_N \Omega^2_{N,\beta} = \frac{(8\pi^2 a_\beta^2)^{N-1}}{\prod_{i=1}^N x_i}. \tag{23}$$

We therefore have four free parameters a_β for the transverse-momentum-dependent part of the LFWAs, given by

$a_{q\bar{q}}$ for the $q\bar{q}$ state, $a_{q\bar{q}g}$ for the $q\bar{q}g$ state,
$a_{q\bar{q}gg}$ for the state $q\bar{q}gg$, and $a_{q\bar{q}\jmath\bar{\jmath}}$ for the $q\bar{q}\jmath\bar{\jmath}$ state.

Let us denote the set of these parameters as $\boldsymbol{A} = \{a_{q\bar{q}}, a_{q\bar{q}g}, a_{q\bar{q}gg}, a_{q\bar{q}\jmath\bar{\jmath}}\}$.

The model (22) suffers from a minor inconvenience: either the DAs or the PDFs have some dependence on the transverse parameters a_β. This means that there is trace of the transverse structure in the collinear part. In principle, this is not an issue, since the dependence can be shown to be just a normalization factor. It is however an unwelcome feature in practical applications. For our purposes, it is important to avoid any dependence in the PDFs from the a_β parameters. We therefore modify the model for $\Omega_{N,\beta}$ to read

$$\Omega_{N,\beta}(x_1,\boldsymbol{k}_{\perp 1},x_2,\boldsymbol{k}_{\perp 2},\ldots,x_N,\boldsymbol{k}_{\perp N}) = \frac{(4\sqrt{2}\pi a_\beta)^{N-1}}{\prod_{i=1}^N x_i}\exp\left(-a_\beta^2\sum_{i=1}^N\frac{\boldsymbol{k}_{\perp i}^2}{x_i}\right). \tag{24}$$

This implies for the normalizations

$$\int [d^2\boldsymbol{k}_\perp]_N \Omega_{N,\beta} = \frac{1}{(2\sqrt{2}\pi a_\beta)^{N-1}}, \tag{25a}$$

$$\int [d^2\boldsymbol{k}_\perp]_N \Omega_{N,\beta}^2 = \frac{1}{\prod_{i=1}^N x_i}. \tag{25b}$$

The net effect is to produce expressions for the PDFs without any dependence of a_β, while the DAs contain these parameters only as global normalization factors. We also note that the PDFs do not depend on the functional forms adopted for the $\Omega_{N,\beta}$ functions, once the normalization conditions in Eqs. (25a) and (25b) are imposed. Furthermore, the choice in Eq. (24) does not introduce a strong model dependence in the fit to the available data for the e.m. form factor: we verified that the fit results are basically identical if we adopt other functional forms, such as, for example, multipolelike functional forms or polynomials multiplied by a Gaussian.

B. Model for the longitudinal-momentum-fraction dependence

For the collinear part, our fundamental building block is the asymptotic expansion of the x dependence of the leading-twist DAs (lowest conformal spin representation of the collinear conformal subgroup [105]), which for the generic N-parton state reads

$$\prod_{i=1}^N x_i^{2j_i-1}, \tag{26}$$

where j_i is the conformal spin of the ith parton, which is $j=1$ for quarks and antiquarks and $j=3/2$ for gluons.

We found that truncating the expansion to the asymptotic expressions for the DAs of the $q\bar{q}$ and $q\bar{q}g$ components leads to poor results for the PDFs. Therefore, for these components, we included the first beyond-asymptotic term in the expansion. For the $q\bar{q}$ state, we modified also the asymptotic expansion, by assuming a variable exponent for the longitudinal-momentum fractions to be fitted to data. We also included the first term orthogonal to this modified asymptotic DA, which is uniquely determined as the lowest-degree nontrivial polynomial in the momentum fractions that is orthogonal to the asymptotic state when integrated with the two-dimensional simplex measure. This is exactly the expansion in Gegenbauer polynomials with variable dimensionality, which has typically a faster convergence than the expansion with fixed dimensionality [7]. For the remaining Fock states, we found that the variable exponents do not change significantly the results of the fit, and therefore we did not introduce these additional parameters. Moreover, for the sea quark contribution, we are not able to distinguish the three LFWAs $\phi^{(1)}_{q\bar{q}j\bar{j}}$, $\phi^{(2)}_{q\bar{q}j\bar{j}}$, and $\phi^{(3)}_{q\bar{q}j\bar{j}}$, as long as we consider unpolarized PDFs with the extant database. We then assume that these three LFWAs share the same dependence on the longitudinal-momentum fractions, though with a different normalization factor. The situation is different for the two-gluon Fock component, for which the LFWA $\phi^{(2)}_{q\bar{q}gg}(x_1,x_2,x_3,x_4)$ is antisymmetric in the last two arguments, whereas the function $\phi^{(1)}_{q\bar{q}gg}(x_1,x_2,x_3,x_4)$ is symmetric. The relative normalizations of the different Fock states are fixed by the requirement on the normalization of the pion state,

$$\langle\pi(P')|\pi(P)\rangle = 2(2\pi)^3P^+\delta(P'^+-P^+)\delta(\boldsymbol{P}'_\perp-\boldsymbol{P}_\perp). \tag{27}$$

Explicitly, the model reads

$$\begin{aligned}\phi^{(1)}_{q\bar{q}}(x_1,x_2) &= N^{(1)}_{q\bar{q}}(x_1x_2)^{\gamma_q}(1+d_{q1}C_2^{(\gamma_q+1/2)}(x_1-x_2))\\ &= N^{(1)}_{q\bar{q}}(x_1x_2)^{\gamma_q}\{1+d_{q1}(1+2\gamma_q)[1+\gamma_q(x_1-x_2)^2-6x_1x_2]\},\end{aligned} \tag{28}$$

$$\phi^{(1)}_{q\bar{q}g}(x_1,x_2,x_3) = N^{(1)}_{q\bar{q}g}x_1x_2x_3^2[1+d_{g1}(3-7x_3)], \tag{29}$$

$$\phi^{(1)}_{q\bar{q}gg} = N^{(1)}_{q\bar{q}gg}x_1x_2(x_3x_4)^2, \tag{30}$$

$$\phi^{(2)}_{q\bar{q}gg} = N^{(2)}_{q\bar{q}gg}x_1x_2x_3x_4(x_3^2-x_4^2), \tag{31}$$

$$\phi^{(1)}_{q\bar{q}j\bar{j}} = N^{(1)}_{q\bar{q}j\bar{j}}x_1x_2x_3x_4, \tag{32}$$

$$\phi^{(2)}_{q\bar{q}j\bar{j}} = N^{(2)}_{q\bar{q}j\bar{j}}x_1x_2x_3x_4, \tag{33}$$

$$\phi^{(3)}_{q\bar{q}j\bar{j}} = N^{(3)}_{q\bar{q}j\bar{j}}x_1x_2x_3x_4, \tag{34}$$

where $C_j^\alpha(x)$ are Gegenbauer polynomials. In Eqs. (28)–(34), the norms are given by

$$N^{(1)}_{q\bar{q}} = \cos(\alpha_1) 4^{\gamma_q} \sqrt{\frac{\Gamma(\frac{5}{2}+2\gamma_q)}{\Gamma(\frac{1}{2})\Gamma(2\gamma_q)}} \{(4\gamma_q+3)[1+4\gamma_q+2d_{q1}(1-\gamma_q)(1+2\gamma_q)] + d^2_{q1}(1+2\gamma_q)^2(3+4\gamma_q+3\gamma_q^2)\}^{-1/2}, \quad (35)$$

$$N^{(1)}_{q\bar{q}g} = 6\sqrt{210}\sin(\alpha_1)\cos(\alpha_2)(18 - 18d_{g1} + 29d^2_{g1})^{-1/2}, \quad (36)$$

$$N^{(1)}_{q\bar{q}gg} = 2\sqrt{\frac{7}{6}} N^{(2)}_{q\bar{q}gg} = 30\sqrt{77}\sin(\alpha_1)\sin(\alpha_2)\cos(\alpha_3), \quad (37)$$

$$N^{(1)}_{q\bar{q}\mathfrak{z}\bar{\mathfrak{z}}} = N^{(2)}_{q\bar{q}\mathfrak{z}\bar{\mathfrak{z}}} = \frac{1}{\sqrt{2}} N^{(3)}_{q\bar{q}\mathfrak{z}\bar{\mathfrak{z}}} = 2\sqrt{35}\sin(\alpha_1)\sin(\alpha_2)\sin(\alpha_3), \quad \text{for } \mathfrak{z}\bar{\mathfrak{z}} = u\bar{u}, d\bar{d}, s\bar{s}, \quad (38)$$

where Γ is the Euler Gamma function.

In summary, we have the following parameters for the longitudinal-momentum-fraction dependence:

- $\alpha_1, \alpha_2, \alpha_3$, for the relative normalization of the different Fock components;
- γ_q, that is the exponent of the modified asymptotic $q\bar{q}$ LFWA;
- d_{q1}; that is the relative normalization between the zeroth and first term of the expansion of the $q\bar{q}$ LFWA.
- d_{g1}, that is the relative normalization between the zeroth and first term of the expansion of the $q\bar{q}g$ LFWA.

Let us denote the set of these parameters as $\mathcal{X} = \{\alpha_1, \alpha_2, \alpha_3, d_{q1}, d_{g1}, \gamma_q\}$.

IV. COLLINEAR PARTON DISTRIBUTION FUNCTIONS

In this section, we apply the model for the pion LFWFs outlined above to the extraction of the pion PDFs from existing measurements.

The model scale is fixed at $\mu_0^2 = 0.7225\ \text{GeV}^2$, well below the charm mass threshold $m_c^2 = 2.04\ \text{GeV}^2$. Moreover, by neglecting electroweak corrections and quark masses, charge symmetry imposes $f^u_{1,\pi^+} = f^{\bar{d}}_{1,\pi^+} = f^d_{1,\pi^-} = f^{\bar{u}}_{1,\pi^-} = 2f^u_{1,\pi^0} = 2f^{\bar{u}}_{1,\pi^0} = 2f^d_{1,\pi^0} = 2f^{\bar{d}}_{1,\pi^0}$. In the following, we will refer to distributions in positively charged pions, using the notation f_1. Assuming also a SU(3)-symmetric sea, i.e., $f^u_1 = f^{\bar{d}}_1 = f^s_1 = f^{\bar{s}}_1$, we end up with three independent PDFs: the total valence contribution f^v_1, the total sea contribution f^S_1, given by

$$f^v_1 = f^{u_v}_1 - f^{d_v}_1 = (f^u_1 - f^{\bar{u}}_1) - (f^d_1 - f^{\bar{d}}_1) = 2f^{u_v}_1,$$
$$f^S_1 = 2f^u_1 + 2f^{\bar{d}}_1 + f^s_1 + f^{\bar{s}}_1 = 6f^u_1, \quad (39)$$

and the gluon contribution f^g_1. The model-independent expressions for the pion PDFs in terms of overlap of LFWAs are collected in Appendix A. With those expressions and the model for the LFWAs built in Sec. III, we obtain the following parametrizations:

$$f^v_1(x,\mu_0^2) = \mathcal{C}^v_{q\bar{q}}(x\bar{x})^{2\gamma_q-1}[1 + d_{q1}(1+2\gamma_q)(1+\gamma_q(x-\bar{x})^2 - 6x\bar{x})]^2 + \mathcal{C}^v_{q\bar{q}g}x\bar{x}^5[3 + 18xd_{g1} - 10\bar{x}d_{g1} + 13d^2_{g1} + 14xd^2_{g1}(x-4\bar{x})] + \mathcal{C}^v_{q\bar{q}gg}x\bar{x}^9 + \sum_{\{\mathfrak{z}\bar{\mathfrak{z}}\}}\mathcal{C}^v_{q\bar{q}\{\mathfrak{z}\bar{\mathfrak{z}}\}}x\bar{x}^5, \quad (40)$$

$$f^g_1(x,\mu_0^2) = \mathcal{C}^g_{q\bar{q}g}(x\bar{x})^3[1 + d_{g1}(3-7x)]^2 + \mathcal{C}^g_{q\bar{q}gg_1}x^3\bar{x}^7 + \mathcal{C}^g_{q\bar{q}gg_2}x\bar{x}^5(5 - 20x - 6x^2 + 52x^3 + 95x^4), \quad (41)$$

$$f^S_1(x,\mu_0^2) = 2\sum_{\{\mathfrak{z}\bar{\mathfrak{z}}\}}\mathcal{C}^S_{q\bar{q}\{\mathfrak{z}\bar{\mathfrak{z}}\}}x\bar{x}^5, \quad (42)$$

where $\bar{x} = 1 - x$ and the $\mathcal{C}$ coefficients are given by

$$\mathcal{C}^v_{q\bar{q}} = (2N^{(1)}_{q\bar{q}})^2, \quad \mathcal{C}^v_{q\bar{q}g} = \frac{1}{15}(N^{(1)}_{q\bar{q}g})^2, \quad \mathcal{C}^v_{q\bar{q}gg} = \frac{1}{315}(N^{(1)}_{q\bar{q}gg})^2, \quad \mathcal{C}^v_{q\bar{q}\{\mathfrak{z}\bar{\mathfrak{z}}\}} = \frac{1}{5}(N^{(1)}_{q\bar{q}\mathfrak{z}\bar{\mathfrak{z}}})^2, \quad (43)$$

$$\mathcal{C}^g_{q\bar{q}g} = \frac{1}{3}(N^{(1)}_{q\bar{q}g})^2, \quad \mathcal{C}^g_{q\bar{q}gg_1} = \frac{2}{105}(N^{(1)}_{q\bar{q}gg})^2, \quad \mathcal{C}^g_{q\bar{q}gg_2} = \frac{1}{4410}(N^{(1)}_{q\bar{q}gg})^2, \quad (44)$$

$$\mathcal{C}^{S}_{q\bar{q}\{\jmath\bar{\jmath}\}} = \frac{1}{10}(N^{(1)}_{q\bar{q}\jmath\bar{\jmath}})^2. \tag{45}$$

The valence number and momentum sum rules are guaranteed by construction, i.e.,

$$\int_0^1 f_1^v(x)dx = 2, \qquad \int_0^1 x(f_1^v(x)+f_1^g(x)+f_1^S(x))dx = 1. \tag{46}$$

A. Fit procedure

The PDF fit of the cross section experimental data has been performed by using the open-source tool xFitter [97]. Technical details about the fit setup can be found in [98]. Here we report only the essential information necessary to reproduce our fit results. In our analysis, we consider DY data from the NA10 [106] and E615 [107] experiments and prompt photon-production data (WA70) [108]. The DY data have been obtained by studying the scattering of a π^- beam off a tungsten target, with the pion beam energy $E_\pi =$ 194 and 286 GeV in the NA10 experiment, and $E_\pi =$ 252 GeV in the E615 experiment. Instead, the prompt photon-production data of the WA70 experiment have been measured by using $\pi^\pm$ beams, with $E_\pi = 280$ GeV, on a proton target. In order to avoid the J/ψ and Υ resonances and the lower edges of phase space, we apply the following cuts: $4.16 < \mu < 7.68$ GeV, and $x_F \geq 0$, where the Feynman variable x_F is defined as $x_F = x_0^\pi - x_0^A$ with $x_0^{\pi(A)}$ the minimum momentum fraction of the active parton in the pion (nucleus) to produce the lepton pair in the final state. The number of data points after the cuts is 91 for the E615 set and 70 for the NA10 set. Including also the prompt photon data, our database consists of a total number of 260 points.

The minimization function is defined as

$$\chi^2 = \sum_i \frac{(E_i - \tilde{t}_i)^2}{(\delta_i^{\text{syst}})^2 + \left(\sqrt{\frac{\tilde{t}_i}{t_i}}\delta_i^{\text{stat}}\right)^2} + \sum_\alpha b_\alpha^2, \tag{47}$$

where the index i runs over the data points and α is the index of the source of correlated error. In Eq. (47) E_i are the measured cross sections with the corresponding systematic and statistical uncertainties δ_i^{syst} and δ_i^{stat}, respectively. Moreover, $\tilde{t}_i = t_i(1 - \sum_\alpha \zeta_{i\alpha} b_\alpha)$ are the theory predictions t_i corrected for the correlated shifts, obtained by taking into account the relative coefficient $\zeta_{i\alpha}$ of the influence of the correlated error source α on the data point i and the nuisance parameter b_α. The nuisance parameters are included in the minimization along with the PDF parameters and contribute to the χ^2 via the penalty term $\sum_\alpha b_\alpha^2$ [98].

B. Fit results

The model parameters to be fitted are the 6 collinear coefficients of the pion PDFs described in Sec. III B. In addition to the initial scale μ_0, we fixed the factorization scale μ_F and the renormalization scale μ_R to $\mu_F = \mu_R = 0.8$ GeV. The minimization of the function (47) is performed by using MINUIT [109]. For the averaged value of the fitted parameters we find

$$\langle d_{q1}\rangle = -0.142, \quad \langle \gamma_q\rangle = 0.639, \quad \langle d_{g1}\rangle = 111.386,$$
$$\langle \alpha_1\rangle = 0.816, \quad \langle \alpha_2\rangle = 1.364, \quad \langle \alpha_3\rangle = 0.554. \tag{48}$$

The reduced chi-squared from a single minimization is $\hat{\chi}^2/N_{\text{d.o.f.}} = 0.88$ for the number of degrees of freedom $N_{\text{d.o.f.}} = 260 - 6 = 254$.

We also repeated the fit by varying the value of the initial scale around $\mu_0 = 0.85$ GeV and we did not observe significant variations in the quality of the fit (the chi-squared varied by less then 1% when changing μ_0 in the range [0.65, 1.05] GeV). The error analysis is performed with the bootstrap method, by fitting an ensemble of 1000 replicas of experimental data varied by using a random Gaussian shift both for the statistic and systematic uncertainties. Furthermore, we took into account the effects of variations of the factorization and renormalization scales by changing the values of μ_F and μ_R replica by replica. In particular, the value of μ_F has been randomly generated from a uniform distribution in the range $[\mu_0/2, \mu_0]$, while μ_R was varied in the range $[\mu_F, 2\mu_0]$, i.e., we explored the regions of $\mu_0/2 \leq \mu_F \leq \mu_0$ and $\mu_0/2 \leq \mu_R \leq 2\mu_0$.

In Fig. 1 we show the results for the pion PDFs at the scales of $\mu^2 = 5$ GeV^2. The light and dark red uncertainty bands are our fit results, corresponding, respectively, to 3σ (99.7%) and 1σ (68%) confidence level (CL). They are compared with the extractions of pion PDFs from other studies. The solid black curves correspond to the best fit of the analysis in Ref. [42] (GRVPI1 solution) and the gray bands refer to the results of the xFitter Collaboration [98]. These analyses and our work were based on the same measurements, with small variations in the database due to different kinematical cuts (we refer to the original works for details). The analysis from the JAM Collaboration [49] is shown by the light blue bands and includes both the DY data and the leading-neutron tagged electroproduction data, taking into account also threshold resummation on DY cross sections at next-to-leading-log accuracy. The yellow bands show a new analysis by Bourrely, Chang, and Peng (BCP) in the framework of the statistical model [44] which extended the database considered in a previous work [45] to include J/ψ-production data. Overall, the modern analyses give compatible results within the relative error bands. The agreement is better for the valence and sea contributions at larger x and for the gluon PDF in the small x region. The difference in shape of our results for the valence PDF in the

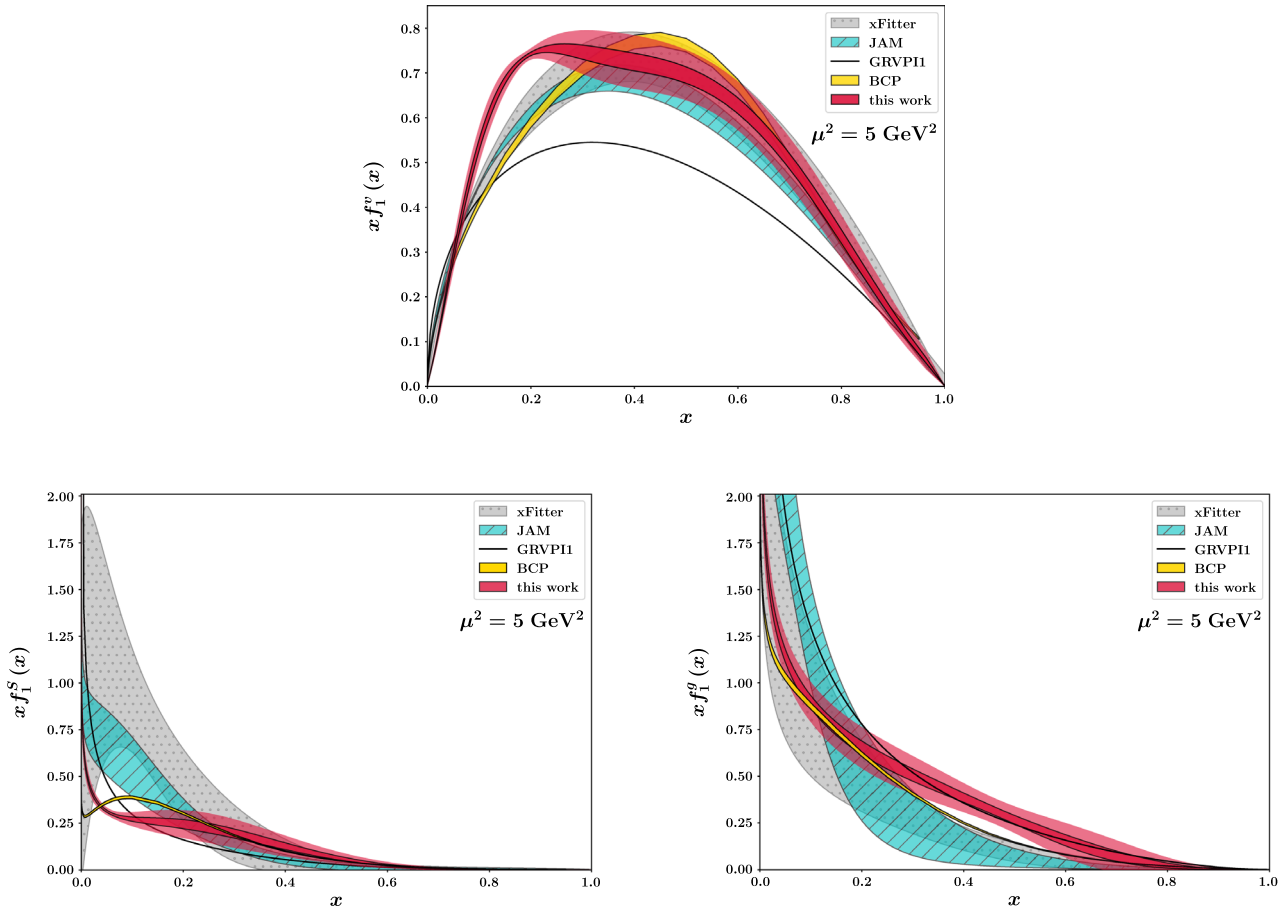

FIG. 1. xf_1 as function of x for the total valence (upper), total sea (bottom left) and gluon (bottom right) contributions at $\mu^2 = 5$ GeV^2. The light (dark) red bands show the results of this work with the 3σ (1σ) uncertainty in comparison with the results from the JAM Collaboration [49] (light blue bands), the analysis of xFitter Collaboration [98] (gray bands), the BCP fit of Ref. [44] (yellow bands), and the GRVPI1 fit [42] (solid black curves).

region $0.05 < x < 0.2$ can be ascribed to a strong correlations between the valence PDF at small x and the gluon PDF at large x. This is peculiar to the LFWF approach. From the explicit expressions for the PDFs in Eqs. (40)–(42), we notice that the valence PDF receives contributions from all Fock states. In particular, the low-x behavior of the valence PDF is influenced by the high-x behavior of the other PDFs. These spurious correlations tend to lessen when the expansion in the Fock space spans a large number of Fock components. However, one has to admit that the extension of the present formalism at higher-order Fock components may become quite cumbersome.

In Fig. 2, we show our results at $\mu^2 = 27$ GeV^2 with light (dark) red bands corresponding to 3σ (1σ) CL. The u quark valence PDF is in very good agreement with the extraction of the E615 experiment [107] which neglected threshold resummation effects as we did in our fit procedure. However, in a seminal paper Aicher, Schäfer, and Vogelsang (ASV) [110] found that corrections from threshold resummation can significantly modify the large-x asymptotic behavior of the valence quark contribution, as shown by the solid cyan curve in Fig. 2.[1] This large-x behavior is reproduced very well from the light-front constituent quark model (LFCQM) predictions of Ref. [8] (green dash-dotted curve), which considered only the $q\bar{q}$ Fock component at the hadronic scale and applied next-to-leading-order evolution to the relevant experimental scale. Analogously, the results of the basis light-front quantization (BLFQ) Collaboration [21] within a light-front model including the $q\bar{q}$ and $q\bar{q}g$ Fock components and the study of Ref. [111] with Bethe-Salpeter wave functions (BSWF) for the $q\bar{q}$ state are consistent with the behavior at large x inferred from the analyses with the threshold resummation. In Fig. 2, we also compare the outcome of our study for the sea and gluon contributions with the BLFQ and BSWF results. While our PDF parametrizations take into account nonperturbative sea and gluon contributions at the initial hadronic scale, the BSWF

[1]The ASV analysis focused mainly on the fit of the valence PDF, using parametrizations for the gluon and sea contribution from other works [43] which are not shown here.

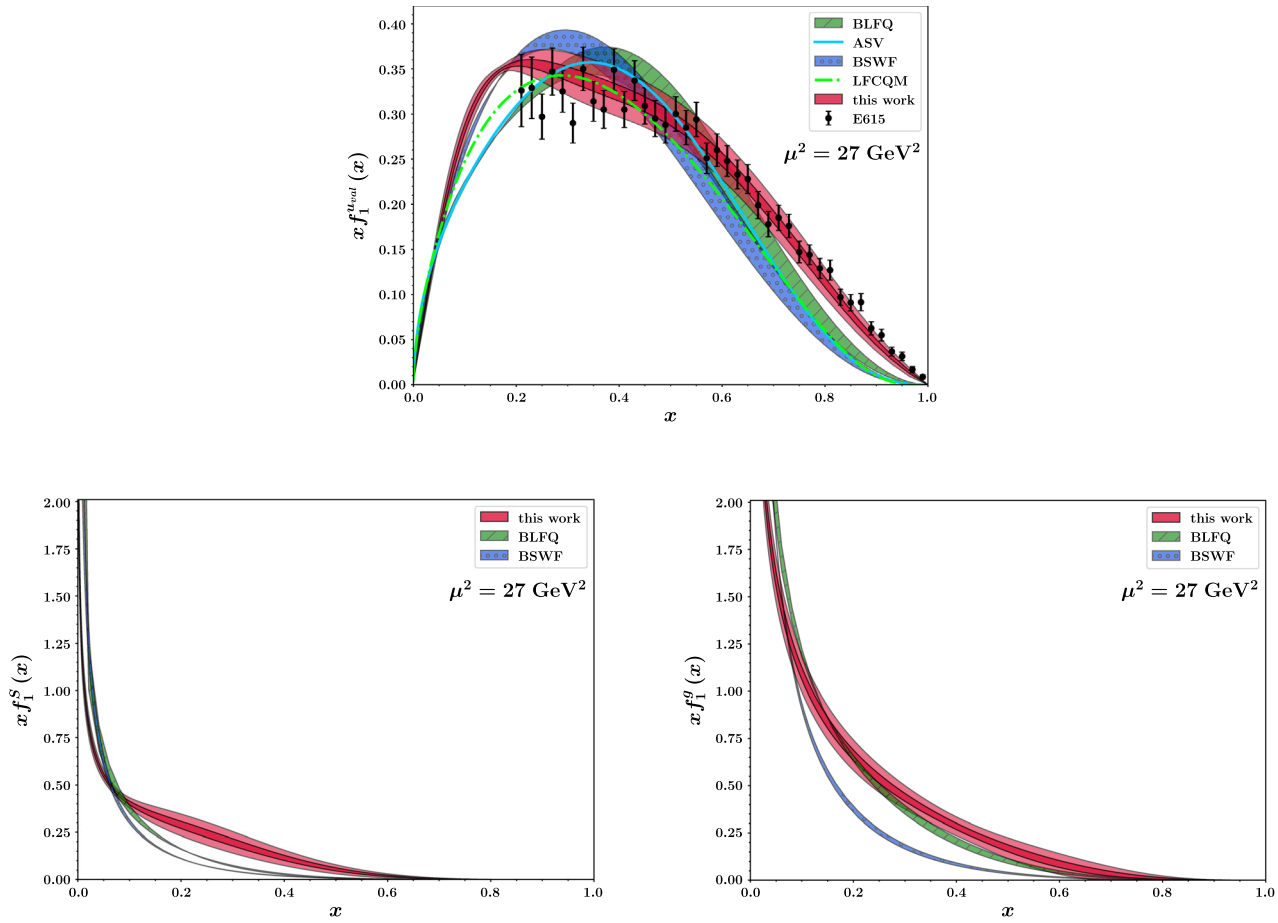

FIG. 2. xf_1 as function of x for the valence u quark (upper), total sea (bottom left) and gluon (bottom right) contributions at $\mu^2 = 27$ GeV^2. The light (dark) red bands show the results of this work with the 3σ (1σ) uncertainty in comparison with the BSWF results from Ref. [112] (blue bands) and the analysis from the BLFQ Collaboration [21] (green bands). For the valence u quark contribution we show also the ASV parametrization of Ref. [110] (cyan solid curve), and the results within the LFCQM of Ref. [8] (green dash-dotted curve), while the data are from the E615 experiment [107].

approach generates both the sea and gluon contributions solely from the scale evolution, and the BLFQ model includes only a dynamical gluon contribution at the initial scale and generates the sea PDF perturbatively. One can clearly appreciate the effects of nonperturbative sea and gluon contributions that result at $x \geq 0.1$ in larger sea PDFs in our analysis, and larger gluon PDFs in our and BLFQ analyses. We also observe a steeper rise at lower values of x in the BLFQ and BSWF models than in our results for the gluon and sea PDFs. Despite the different shapes of the PDFs in our fit and the BSWF and BLFQ analyses, the first moments of the PDFs, defined as $\int \mathrm{d}x\, x f_1$, are well compatible within the error bars, as shown in Table I.

In the same table, we also collect the results of other studies at different scales. We observe that at the initial scale $\mu^2 = 1.69$ GeV^2 of the xFitter and JAM analyses, the values for the gluon are larger in our model and JAM input than in xFitter, although they are still consistent within the error bar. The same trend remains at higher scales after evolution. Comparing our results with the recent BCP extractions, we find a remarkable agreement for the valence moments, while our values for the sea contribution are smaller, mainly because of the different behavior of the sea PDFs at $x \lesssim 0.1$ as shown, for example, in Fig. 1 for the results at $\mu^2 = 5$ GeV^2. The lattice calculations for the valence contribution obtained systematically smaller values than the phenomenological analyses, while the lattice values for the gluon changed significantly going from the analysis of Ref. [113] using quenched QCD and a large 800 MeV pion mass to the study of Ref. [114] with clover fermion action and 450 MeV pion mass. We also report the result for the gluon contribution of a recent calculation [116] which presents for the first time the decomposition into gluon and quark contributions. In particular, they calculated the total $u + d$, s and c contributions, from which we cannot reconstruct the separate valence and sea

TABLE I. Results from this work (gray rows) for the momentum fractions of the pion carried by the valence, sea, and gluon PDFs at different scales μ^2, in comparison with other phenomenological extractions, model calculations, and lattice-QCD analyses.

	μ^2 GeV^2	$\langle x f_1^v \rangle$	$\langle x f_1^S \rangle$	$\langle x f_1^g \rangle$
JAM [49]	1.61	0.53 ± 0.02	0.14 ± 0.04	0.34 ± 0.06
BLFQ [21]	1.69	0.536	0.069	0.395
JAM [48]	1.69	0.54 ± 0.01	0.16 ± 0.02	0.30 ± 0.02
xFitter [98]	1.69	0.55 ± 0.06	0.26 ± 0.15	0.19 ± 0.16
This work	1.69	0.58 ± 0.03	0.09 ± 0.04	0.33 ± 0.06
Latt1 [113]	4			$0.37 \pm 0.08 \pm 0.12$
Latt2 [114]	4			0.61 ± 0.09
Latt3 [115]	4	0.415 ± 0.0212		
Latt4 [36]	4	0.376 ± 0.112		
Latt5 [116]	4			$0.52 \pm 0.11^{+0.02}_{-0.00}$
BLFQ [21]	4	0.484	0.094	0.421
BSWF [112]	4	0.47 ± 0.02	0.11 ± 0.02	0.41 ± 0.02
xFitter [98]	4	0.50 ± 0.05	0.25 ± 0.13	0.25 ± 0.13
This work	4	0.52 ± 0.03	0.11 ± 0.03	0.37 ± 0.05
JAM [48]	5	0.48 ± 0.01	0.17 ± 0.01	0.35 ± 0.02
xFitter [98]	5	0.49 ± 0.05	0.25 ± 0.12	0.26 ± 0.13
BCP [44]	5	0.50 ± 0.01	0.19 ± 0.012	0.31 ± 0.002
This work	5	0.51 ± 0.03	0.12 ± 0.03	0.37 ± 0.05
BLFQ [21]	10	0.446	0.115	0.439
JAM [48]	10	0.44 ± 0.01	0.19 ± 0.01	0.37 ± 0.02
xFitter [98]	10	0.46 ± 0.02	0.22 ± 0.08	0.31 ± 0.06
BCP [44]	10	0.48 ± 0.08	0.21 ± 0.012	0.33 ± 0.015
This work	10	0.48 ± 0.03	0.13 ± 0.02	0.39 ± 0.05
Latt4 [36]	27	0.330 ± 0.018		
BLFQ [21]	27	0.414	0.132	0.451
BSWF [112]	27	0.41 ± 0.04	0.14 ± 0.02	0.45 ± 0.02
xFitter [98]	27	0.42 ± 0.04	0.25 ± 0.10	0.32 ± 0.10
This work	27	0.45 ± 0.02	0.15 ± 0.02	0.40 ± 0.04

contributions. Their results for the sum over all quark flavors is $\sum_q \langle x f_1^q \rangle = 0.68 \pm 0.05^{+0.00}_{-0.03}$, while the sum of all contributions amounts to $1.20 \pm 0.13^{+0.00}_{-0.03}$, compatible with the expected value of 1 within two sigma. There exists also a new lattice study of the x dependence of the gluon PDF at $\mu^2 = 4$ GeV^2 [38]. It reports the results for $x f_1^g(x)$ normalized to unity and gives indications that future lattice studies with improved precision and systematic control may help to provide best determinations of the gluon content in the pion when combined in global-fit analyses.

V. ELECTROMAGNETIC FORM FACTOR

As the PDFs, the e.m. form factor can be written in terms of an overlap of LFWAs, see Appendix B. The nondiagonal matrix elements prevent one from using Eq. (23) in the computation. In principle, one can obtain full analytical expression for the form factor, although it is long and rather uninformative. We present here the model result in terms of the contributions of the different Fock states and in the implicit integral form, which allows for compact expressions, i.e.,

$$F_\pi(Q^2) = F_{\pi,q\bar{q}}(Q^2) + F_{\pi,q\bar{q}g}(Q^2) + F_{\pi,q\bar{q}gg}(Q^2) + \sum_{\{\jmath\bar{\jmath}\}} F_{\pi,q\bar{q}\{\jmath\bar{\jmath}\}}(Q^2), \tag{49}$$

with

$$F_{\pi,q\bar{q}}(Q^2) = \frac{1}{2}\mathcal{C}^v_{q\bar{q}} \int_0^1 dx\,(x\bar{x})^{2\gamma_q-1}[1 + d_{q1}(1+2\gamma_q)(1+\gamma_q(x-\bar{x})^2 - 6x\bar{x})]^2 \exp\left[-a^2_{q\bar{q}}Q^2\frac{\bar{x}}{2x}\right],$$
$$F_{\pi,q\bar{q}g}(Q^2) = \frac{1}{2}\mathcal{C}^v_{q\bar{q}g} \int_0^1 dx\,x\bar{x}^5(3 + 18xd_{g1} - 10\bar{x}d_{g1} + 13d^2_{g1} + 14xd^2_{g1}(x-4\bar{x}))\exp\left[-a^2_{q\bar{q}g}Q^2\frac{\bar{x}}{2x}\right],$$
$$F_{\pi,q\bar{q}gg}(Q^2) = \frac{1}{2}\mathcal{C}^v_{q\bar{q}gg} \int_0^1 dx\,x\bar{x}^9 \exp\left[-a^2_{q\bar{q}gg}Q^2\frac{\bar{x}}{2x}\right],$$
$$F_{\pi,q\bar{q}\{\jmath\bar{\jmath}\}}(Q^2) = \frac{1}{2}\mathcal{C}^v_{q\bar{q}\jmath\bar{\jmath}} \int_0^1 dx\,x\bar{x}^5 \exp\left[-a^2_{q\bar{q}\jmath\bar{\jmath}}Q^2\frac{\bar{x}}{2x}\right], \tag{50}$$

where $Q^2 = -q^2 > 0$ and $q = p' - p$ the four-momentum transfer. The form factor (FF) is normalized as $F_\pi(Q^2 = 0) = 1$, consistent with the valence sum rule. The collinear parameters $\mathcal{X}$ of the LFWAs have been determined by the fit of the pion PDF. The only free parameters in the fit of the pion FF are those entering in the $\Omega_{N,\beta}$ functions of Eq. (22), i.e., the set $\boldsymbol{A}$.

A. Fit procedure

The available experimental data of the pion e.m. form factor come from different extractions exploring various kinematic regions. The CERN measurements of $\pi - e$ scattering experiments [86] provide data for the square of the pion e.m. form factor in the range $0.015 \le Q^2 \le 0.253$ GeV^2. The extension to larger values of Q^2 requires the use of pion electroproduction from a nucleon target (Sullivan process [117]). This process has been exploited for the extraction of F_π at JLab [92,94,96] and DESY [89]. Combining all the datasets, we have 100 experimental points in a Q^2 range from 0.015 to 9.77 GeV^2.

As in the case of the PDF, we use the bootstrap replica method to propagate the experimental uncertainties to our final results. A detailed explanation on the inner workings of the method and examples for its application to extractions involving multiple datasets with systematic errors can be found in Ref. [118]. Moreover, as detailed in Ref. [118], the bootstrap technique is useful also when one wants to propagate the uncertainties associated with parameters of the model that are not directly free fitting variables. In our case, these are the parameters entering the collinear part of the LFWAs. The general logic of the fit procedure is as follows: from the PDF extraction, we obtained a set of $n = 1000$ vectors of parameters, one for each of the replicas of the data used for PDF extraction. Then, for each bootstrap cycle in the form-factor fit, we generate a replica of the data and sample (uniformly) a vector of PDF parameters from the set generated in the PDF fit. We then perform the fit of the form factor computed with the sampled PDF parameters and the free a_β parameters. The minimization function is the bootstrap χ^2_k for the kth bootstrap replica, i.e.,

$$\chi^2_k = \sum_{j=1}^{n_{\rm set}} \sum_{i=1}^{n_{d,{\rm set}_j}} \frac{(F_\pi^{\mathcal{X}_k}(Q^2) - d_{ijk})^2}{\sigma^2_{ijk}}, \tag{51}$$

where $n_{d,{\rm set}_j}$ is the number of data in the jth dataset, $n_{\rm set}$ is the total number of dataset, and $F_\pi^{\mathcal{X}_k}(Q^2)$ is the pion e.m. form factor computed using the kth uniformly sampled vector of collinear parameters $\mathcal{X}_k$. The bootstrap quantities are defined as

$$d_{ijk} = (1+\delta_{ik})(d_{ij} + \sigma_{ijk}) = (1+\delta_{ik})(d_{ij} + r_{ijk}\sigma_{ij}), \tag{52}$$

where d_{ij} and σ_{ij} are the experimental data points and error, respectively, δ_{ik} is a random value extracted from the distribution for the systematic error of set i, and r_{ijk} is a random number extracted from a normal distribution.

After the minimization is performed for all bootstrap replicas, we can use the results to construct the multidimensional probability distribution for the parameters and crucially extract the correlation coefficients for all pairs of parameters.

The set of transverse parameters $\boldsymbol{A}$ contains four distinct elements. However, due to the extremely small norm of the $q\bar{q}g$ state as obtained from the PDF fit, the form-factor fit is not sensitive to the value of $a_{q\bar{q}g}$. We will therefore exclude this parameter from the fit by fixing it arbitrarily to 1 GeV^{-1}. The specific value is inconsequential, since ultimately the corresponding contribution to the form factor is irrelevant.

B. Fit results

Including systematic uncertainties for different datasets and the sampling for the nonfitted parameters, it implies that the probability distribution for the chi-squared can be substantially different from the standard chi-squared distribution. To estimate the confidence level for the value of the single minimization $\hat{\chi}^2$, we perform a second bootstrap against fake data generated from the average value of parameters extracted from the "true" bootstrap run. The set of chi-squared obtained from this second bootstrap represents an estimation of the confidence interval (CI) for the

TABLE II. Full correlation table for the fitted parameters. On the diagonals are shown the standard deviations of the parameters. All the off-diagonal elements represent the linear correlation coefficients of the corresponding pair of parameters.

	$a^2_{q\bar{q}}$	$a^2_{q\bar{q}gg}$	$a^2_{q\bar{q}s\bar{s}}$	d_{1g}	d_{1q}	γ_q	α_1	α_2	α_3
$a^2_{q\bar{q}}$	0.356	−0.593	−0.656	0.067	−0.050	−0.056	0.056	−0.088	−0.046
$a^2_{q\bar{q}gg}$	−0.593	0.080	0.484	−0.381	0.069	0.099	−0.288	0.599	−0.161
$a^2_{q\bar{q}s\bar{s}}$	−0.656	0.484	0.309	−0.181	0.076	0.081	−0.177	0.273	−0.011
d_{1g}	0.067	−0.381	−0.181	220.545	−0.260	−0.253	0.277	−0.495	0.002
d_{1q}	−0.050	0.069	0.076	−0.260	0.047	0.982	−0.108	0.048	0.245
γ_q	−0.056	0.099	0.081	−0.253	0.982	0.100	−0.083	0.079	0.195
α_1	0.056	−0.288	−0.177	0.277	−0.108	−0.083	0.018	−0.635	−0.605
α_2	−0.088	0.599	0.273	−0.495	0.048	0.079	−0.635	0.202	0.054
α_3	−0.046	−0.161	−0.011	0.002	0.245	0.195	−0.605	0.054	0.082

chi-squared computed from a single minimization of our model, without replica of the data. Details on the theory behind this procedure are given in [118]. We obtain for the reduced chi-squared $\hat{\chi}^2/N_{\text{d.o.f.}}$,

$$\hat{\chi}^2/N_{\text{d.o.f.}} = 1.194, \qquad \text{CI}\,68\% = [0.890, 1.204], \qquad \text{CI}\,99\% = [0.682, 1.593], \tag{53}$$

for $N_{\text{d.o.f.}} = N - N_A = 97$, with the total number of data $N = 100$ and the number of fitting parameters $N_A = 3$. This shows that the single minimization $\hat{\chi}^2$ is inside the 68% confidence interval.

For the minimized parameters, we find (in units of GeV^{-2})

$$a^2_{q\bar{q}} = 1.559, \qquad a^2_{q\bar{q}gg} = 0.509, \qquad a^2_{q\bar{q}s\bar{s}} = 0.796. \tag{54}$$

In Table II we show the correlation matrix of the parameters. We notice a very large error for the d_{1g} parameter. This is because the PDF fit prefers configurations with very small norm for the $q\bar{q}g$ component, and therefore it is almost insensitive to the d_{1g} parameter. Moreover, the strong correlations between the transverse parameters are expected. These parameters correspond to the width of the x-dependent Gaussian functions of the various terms in Eq. (50) and their contributions to the form factor are modulated only by the integral over x.

In Fig. 3, we show the results for the square of the pion e.m. form factor obtained from the fit with the bootstrap method. The inner (dark blue) band represents the 68% uncertainty, while the external (light blue) band shows the 99.7% uncertainty. Agreement with the different datasets is qualitatively evident. We stress that the two bands incorporate the error propagation of the PDF parameters, representing therefore more than just the experimental uncertainty on the form factor.

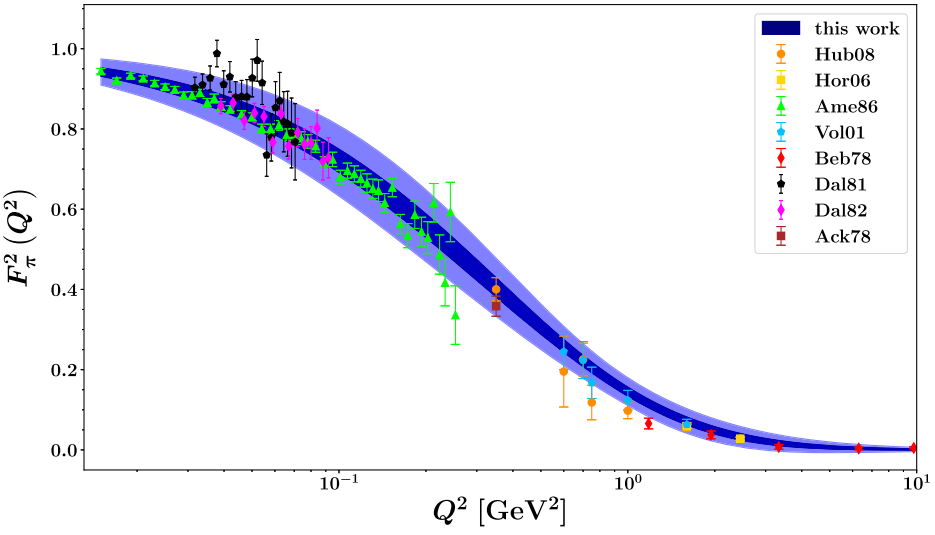

FIG. 3. Fit results for the square of the pion electromagnetic form factor as function of Q^2. The dark (light) blue band shows the 68% (99.7%) of the replicas. The experimental data correspond to Hub08 [96], Hor06 [94], Ame86 [86], Vol01 [92], Beb78 [89], Dal82 [83,84], Ack78 [91].

VI. CONCLUSIONS

In this work, we presented an extraction of the pion parton distribution functions and pion electromagnetic form factor using a new parametrization for the pion light-front wave functions. At the initial scale of the model, we considered the $q\bar{q}$, $q\bar{q}q\bar{q}$, $q\bar{q}g$, and $q\bar{q}gg$ components of the pion state, spanning a larger basis of states than in existing light-front model calculations. We inferred the parametrization in the longitudinal-momentum space from the pion distribution amplitudes, while we used a modified x-dependent Gaussian ansatz for the transverse-momentum-dependent part. The functional form of the LFWF for each parton configuration was chosen so that the fit of the collinear PDFs does not contain any spurious dependence of the parameters in the transverse-momentum space. The collinear parameters were fitted to available Drell-Yan and photon-production data within the xFitter framework, using the bootstrap method for the error analysis. The quality of the fit of the pion PDFs is comparable to existing extractions in literature with the main differences for the gluon and sea contributions that are less constrained by the available data. However, comparing our results for the pion PDFs with other model calculations where the gluon and/or the sea contributions are generated only through perturbative evolution, we can appreciate the effects of including nonperturbative sea and gluon contributions in the light-front Fock expansion at the hadronic scale. Once the collinear parameters were determined, we were able to fix the residual transverse-momentum-dependent parameters from a fit to the available data on the pion electromagnetic form factor. The fit was performed with a bootstrap method that incorporates the propagation of the uncertainties for the collinear parameters in the error band of the electromagnetic form factor and provides the correlation matrix of the whole set of collinear and transverse parameters.

The procedure outlined in this work represents a proof-of-principle for a unified description of hadron distribution functions from inclusive and exclusive processes that involve both the longitudinal- and transverse-momentum motion of partons inside hadrons. The final goal will be to include also the transverse-momentum-dependent parton distributions (TMDs) and generalized parton distributions (GPDs) in a global fit, capitalizing on the extended database expected from upcoming experiments at JLab, COMPASS++/AMBER, and future electron-ion colliders and going a step further than existing analysis that so far considered only PDFs and TMDs simultaneously [119] or focused on TMDs [120,121] and GPDs [19] separately.

ACKNOWLEDGMENTS

We are grateful to V. Bertone and I. Novikov for valuable discussions and for the help in using the xFitter framework. We thank G. Bozzi for a careful reading of the manuscript and useful comments. We acknowledge all the groups who provided us with their results for the pion PDFs at different scales, not always available in the original publications: in particular, D. Binosi for the BSWF results, C. Bourrelly and J.-C. Peng for the BDP results, J. Lan for the BLFQ results, P. Barry for the JAM extractions, and I. Novikov for the xFitter results. The work of B. P. and S. V. is supported by the European Union's Horizon 2020 programme under Grant Agreement No. 824093 (STRONG2020).

APPENDIX A: LFWA OVERLAP REPRESENTATION OF THE PION PARTON DISTRIBUTION FUNCTION

In this appendix, we report the overlap representation of the pion PDF in terms of the LFWAs corresponding to the parton configuration with zero partons' orbital angular momentum in Eqs. (4)–(7). We can write the pion PDFs as the sum of the contributions from each parton configuration, i.e.,

$$f_1^v(x) = f_{1,q\bar{q}}^v(x) + f_{1,q\bar{q}g}^v(x) + f_{1,q\bar{q}gg}^v(x) + \sum_{\{\jmath\bar{\jmath}\}} f_{1,q\bar{q}\{\jmath\bar{\jmath}\}}^v(x), \tag{A1}$$

$$f_1^g(x) = f_{1,q\bar{q}g}^g(x) + f_{1,q\bar{q}gg}^g(x), \tag{A2}$$

$$f_1^S(x) = 2\sum_{\{\jmath\bar{\jmath}\}} f_{1,q\bar{q}\{\jmath\bar{\jmath}\}}^S(x), \tag{A3}$$

where

$$f_{1,q\bar{q}}^v(x) = 4\int d[1]d[2]\sqrt{x_1x_2}\,\delta(x-x_1)|\psi_{q\bar{q}}^{(1)}(1,2)|^2, \tag{A4}$$

$$f_{1,q\bar{q}g}^v(x) = 4\int d[1]d[2]d[3]\sqrt{x_1x_2x_3}\,\delta(x-x_1)|\psi_{q\bar{q}g}^{(1)}(1,2,3)|^2, \tag{A5}$$

$$f_{1,q\bar{q}gg}^v(x) = 16\int d[1]d[2]d[3]d[4]\sqrt{x_1x_2x_3x_4}\,\delta(x-x_1)[|\psi_{q\bar{q}gg}^{(1)}(1,2,3,4)|^2 + |\psi_{q\bar{q}gg}^{(2)}(1,2,3,4)|^2], \tag{A6}$$

$$f^{v}_{1,q\bar{q}\{s\bar{s}\}}(x) = 8\int d[1]d[2]d[3]d[4]\sqrt{x_1x_2x_3x_4}\,\delta(x-x_1)\left[|\psi^{(1)}_{q\bar{q}s\bar{s}}(1,2,3,4)|^2+|\psi^{(2)}_{q\bar{q}s\bar{s}}(1,2,3,4)|^2+\frac{1}{2}|\psi^{(3)}_{q\bar{q}s\bar{s}}(1,2,3,4)|^2\right], \tag{A7}$$

$$f^{g}_{1,q\bar{q}g}(x) = 2\int \mathrm{d}[1]\mathrm{d}[2]\mathrm{d}[3]\sqrt{x_1x_2x_3}\,\delta(x-x_3)|\psi^{(1)}_{q\bar{q}g}(1,2,3)\Big|^2 \tag{A8}$$

$$f^{g}_{1,q\bar{q}gg}(x) = 16\int d[1]d[2]d[3]d[4]\sqrt{x_1x_2x_3x_4}\,\delta(x-x_3)[|\psi^{(1)}_{q\bar{q}gg}(1,2,3,4)|^2+|\psi^{(2)}_{q\bar{q}gg}(1,2,3,4)|^2], \tag{A9}$$

$$f^{S}_{1,q\bar{q}\{s\bar{s}\}}(x) = 4\int d[1]d[2]d[3]d[4]\sqrt{x_1x_2x_3x_4}\,\delta(x-x_3)\left[|\psi^{(1)}_{q\bar{q}s\bar{s}}(1,2,3,4)|^2+|\psi^{(2)}_{q\bar{q}s\bar{s}}(1,2,3,4)|^2+\frac{1}{2}|\psi^{(3)}_{q\bar{q}s\bar{s}}(1,2,3,4)|^2\right]. \tag{A10}$$

APPENDIX B: LFWA OVERLAP REPRESENTATION OF THE PION FORM FACTOR

In this appendix, we report the overlap representation of the pion form factor in terms of the LFWAs corresponding to the parton configuration with zero partons' orbital angular momentum in Eqs. (4)–(7). The contributions from each parton configuration in Eq. (49) read

$$F_{\pi,q\bar{q}}(Q^2) = 2\int d[1]d[2]\sqrt{x_1x_2}\,\psi^{*(1)}_{q\bar{q}}(x_1,x_2,\boldsymbol{k}_{\perp1}+(1-x_1)\boldsymbol{q}_\perp,\boldsymbol{k}_{\perp2}-x_2\boldsymbol{q}_\perp)\psi^{(1)}_{q\bar{q}}(1,2), \tag{B1}$$

$$F_{\pi,q\bar{q}g}(Q^2) = 2\int d[1]d[2]d[3]\sqrt{x_1x_2x_3}\,\psi^{*(1)}_{q\bar{q}g}(x_1,x_2,x_3,\boldsymbol{k}_{\perp1}+(1-x_1)\boldsymbol{q}_\perp,\boldsymbol{k}_{\perp2}-x_2\boldsymbol{q}_\perp,\boldsymbol{k}_{\perp3}-x_3\boldsymbol{q}_\perp)\psi^{(1)}_{q\bar{q}g}(1,2,3), \tag{B2}$$

$$\begin{aligned}F_{\pi,q\bar{q}gg}(Q^2) = 4\int d[1]d[2]d[3]d[4]\sqrt{x_1x_2x_3x_4}\\ \times[\psi^{*(1)}_{q\bar{q}gg}(x_1,x_2,x_3,x_4,\boldsymbol{k}_{\perp1}+(1-x_1)\boldsymbol{q}_\perp,\boldsymbol{k}_{\perp2}-x_2\boldsymbol{q}_\perp,\boldsymbol{k}_{\perp3}-x_3\boldsymbol{q}_\perp,\boldsymbol{k}_{\perp4}-x_4\boldsymbol{q}_\perp)\psi^{(1)}_{q\bar{q}gg}(1,2,3,4)\\ +\psi^{*(1)}_{q\bar{q}gg}(x_1,x_2,x_4,x_3,\boldsymbol{k}_{\perp1}+(1-x_1)\boldsymbol{q}_\perp,\boldsymbol{k}_{\perp2}-x_2\boldsymbol{q}_\perp,\boldsymbol{k}_{\perp4}-x_4\boldsymbol{q}_\perp,\boldsymbol{k}_{\perp3}-x_3\boldsymbol{q}_\perp)\psi^{(1)}_{q\bar{q}gg}(1,2,3,4)\\ +\psi^{*(2)}_{q\bar{q}gg}(x_1,x_2,x_3,x_4,\boldsymbol{k}_{\perp1}+(1-x_1)\boldsymbol{q}_\perp,\boldsymbol{k}_{\perp2}-x_2\boldsymbol{q}_\perp,\boldsymbol{k}_{\perp3}-x_3\boldsymbol{q}_\perp,\boldsymbol{k}_{\perp4}-x_4\boldsymbol{q}_\perp)\psi^{(2)}_{q\bar{q}gg}(1,2,3,4)\\ -\psi^{*(2)}_{q\bar{q}gg}(x_1,x_2,x_4,x_3,\boldsymbol{k}_{\perp1}+(1-x_1)\boldsymbol{q}_\perp,\boldsymbol{k}_{\perp2}-x_2\boldsymbol{q}_\perp,\boldsymbol{k}_{\perp4}-x_4\boldsymbol{q}_\perp,\boldsymbol{k}_{\perp3}-x_3\boldsymbol{q}_\perp)\psi^{(2)}_{q\bar{q}gg}(1,2,3,4)],\end{aligned} \tag{B3}$$

$$\begin{aligned}F_{\pi,q\bar{q}\{s\bar{s}\}}(Q^2) = 4\int d[1]d[2]d[3]d[4]\sqrt{x_1x_2x_3x_4}\\ \times[\psi^{*(1)}_{q\bar{q}s\bar{s}}(x_1,x_2,x_3,x_4,\boldsymbol{k}_{\perp1}+(1-x_1)\boldsymbol{q}_\perp,\boldsymbol{k}_{\perp2}-x_2\boldsymbol{q}_\perp,\boldsymbol{k}_{\perp3}-x_3\boldsymbol{q}_\perp,\boldsymbol{k}_{\perp4}-x_4\boldsymbol{q}_\perp)\psi^{(1)}_{q\bar{q}s\bar{s}}(1,2,3,4)\\ +\psi^{*(2)}_{q\bar{q}s\bar{s}}(x_1,x_2,x_3,x_4,\boldsymbol{k}_{\perp1}+(1-x_1)\boldsymbol{q}_\perp,\boldsymbol{k}_{\perp2}-x_2\boldsymbol{q}_\perp,\boldsymbol{k}_{\perp3}-x_3\boldsymbol{q}_\perp,\boldsymbol{k}_{\perp4}-x_4\boldsymbol{q}_\perp)\psi^{(2)}_{q\bar{q}s\bar{s}}(1,2,3,4)\\ +\frac{1}{2}\psi^{*(3)}_{q\bar{q}s\bar{s}}(x_1,x_2,x_3,x_4,\boldsymbol{k}_{\perp1}+(1-x_1)\boldsymbol{q}_\perp,\boldsymbol{k}_{\perp2}-x_2\boldsymbol{q}_\perp,\boldsymbol{k}_{\perp3}-x_3\boldsymbol{q}_\perp,\boldsymbol{k}_{\perp4}-x_4\boldsymbol{q}_\perp)\psi^{(3)}_{q\bar{q}s\bar{s}}(1,2,3,4)].\end{aligned} \tag{B4}$$

[1] S. J. Brodsky, H.-C. Pauli, and S. S. Pinsky, Quantum chromodynamics and other field theories on the light cone, Phys. Rep. **301**, 299 (1998).

[2] X.-d. Ji, J.-P. Ma, and F. Yuan, Classification and asymptotic scaling of hadrons' light cone wave function amplitudes, Eur. Phys. J. C **33**, 75 (2004).

[3] C. Lorcé, B. Pasquini, and M. Vanderhaeghen, Unified framework for generalized and transverse-momentum dependent parton distributions within a 3Q light-cone picture of the nucleon, J. High Energy Phys. 05 (2011) 041.

[4] J. P. B. C. de Melo, T. Frederico, E. Pace, and G. Salmè, Space-like and time-like pion electromagnetic form-factor and Fock state components within the light-front dynamics, Phys. Rev. D **73**, 074013 (2006).

[5] J. P. B. C. de Melo, T. Frederico, E. Pace, S. Pisano, and G. Salmè, Time- and spacelike nucleon electromagnetic form

factors beyond relativistic constituent quark models, Phys. Lett. B **671**, 153 (2009).
[6] T. Frederico, E. Pace, B. Pasquini, and G. Salmè, Pion generalized parton distributions with covariant and light-front constituent quark models, Phys. Rev. D **80**, 054021 (2009).
[7] L. Chang, I. C. Cloet, J. J. Cobos-Martinez, C. D. Roberts, S. M. Schmidt, and P. C. Tandy, Imaging Dynamical Chiral Symmetry Breaking: Pion Wave Function on the Light Front, Phys. Rev. Lett. **110**, 132001 (2013).
[8] B. Pasquini and P. Schweitzer, Pion transverse momentum dependent parton distributions in a light-front constituent approach, and the Boer-Mulders effect in the pion-induced Drell-Yan process, Phys. Rev. D **90**, 014050 (2014).
[9] T. Gutsche, V. E. Lyubovitskij, I. Schmidt, and A. Vega, Pion light-front wave function, parton distribution and the electromagnetic form factor, J. Phys. G **42**, 095005 (2015).
[10] C. Lorcé, B. Pasquini, and P. Schweitzer, Transverse pion structure beyond leading twist in constituent models, Eur. Phys. J. C **76**, 415 (2016).
[11] N. Chouika, C. Mezrag, H. Moutarde, and J. Rodríguez-Quintero, A Nakanishi-based model illustrating the covariant extension of the pion GPD overlap representation and its ambiguities, Phys. Lett. B **780**, 287 (2018).
[12] A. Bacchetta, S. Cotogno, and B. Pasquini, The transverse structure of the pion in momentum space inspired by the AdS/QCD correspondence, Phys. Lett. B **771**, 546 (2017).
[13] G. F. de Teramond, T. Liu, R. S. Sufian, H. G. Dosch, S. J. Brodsky, and A. Deur (HLFHS Collaboration), Universality of Generalized Parton Distributions in Light-Front Holographic QCD, Phys. Rev. Lett. **120**, 182001 (2018).
[14] A. Watanabe, T. Sawada, and M. Huang, Extraction of gluon distributions from structure functions at small x in holographic QCD, Phys. Lett. B **805**, 135470 (2020).
[15] J. Lan, C. Mondal, S. Jia, X. Zhao, and J. P. Vary, Parton Distribution Functions from a Light Front Hamiltonian and QCD Evolution for Light Mesons, Phys. Rev. Lett. **122**, 172001 (2019).
[16] W. Qian, S. Jia, Y. Li, and J. P. Vary, Light mesons within the basis light-front quantization framework, Phys. Rev. C **102**, 055207 (2020).
[17] S. Bastami, L. Gamberg, B. Parsamyan, B. Pasquini, A. Prokudin, and P. Schweitzer, The Drell-Yan process with pions and polarized nucleons, J. High Energy Phys. 02 (2021) 166.
[18] K. Raya, Z.-F. Cui, L. Chang, J.-M. Morgado, C. D. Roberts, and J. Rodriguez-Quintero, Revealing pion and kaon structure via generalised parton distributions, Chin. Phys. C **46**, 013105 (2022).
[19] J. M. M. Chavez, V. Bertone, F. De Soto Borrero, M. Defurne, C. Mezrag, H. Moutarde, J. Rodríguez-Quintero, and J. Segovia, Pion generalized parton distributions: A path toward phenomenology, Phys. Rev. D **105**, 094012 (2022).
[20] M. Li, Y. Li, G. Chen, T. Lappi, and J. P. Vary, Light-front wavefunctions of mesons by design, Eur. Phys. J. C **82**, 1045 (2022).
[21] J. Lan, K. Fu, C. Mondal, X. Zhao, and J. P. Vary (BLFQ), Light mesons with one dynamical gluon on the light front, Phys. Lett. B **825**, 136890 (2022).
[22] E. Ydrefors, W. de Paula, J. H. A. Nogueira, T. Frederico, and G. Salmé, Pion electromagnetic form factor with Minkowskian dynamics, Phys. Lett. B **820**, 136494 (2021).
[23] W. de Paula, E. Ydrefors, J. H. Nogueira Alvarenga, T. Frederico, and G. Salmè, Parton distribution function in a pion with Minkowskian dynamics, Phys. Rev. D **105**, L071505 (2022).
[24] Y. Li, P. Maris, and J. P. Vary, Chiral sum rule on the light front and the 3D image of the pion, Phys. Lett. B **836**, 137598 (2023).
[25] Y. Lu, L. Chang, K. Raya, C. D. Roberts, and J. Rodríguez-Quintero, Proton and pion distribution functions in counterpoint, Phys. Lett. B **830**, 137130 (2022).
[26] Z. F. Cui, M. Ding, J. M. Morgado, K. Raya, D. Binosi, L. Chang, F. De Soto, C. D. Roberts, J. Rodríguez-Quintero, and S. M. Schmidt, Emergence of pion parton distributions, Phys. Rev. D **105**, L091502 (2022).
[27] Z. F. Cui, M. Ding, J. M. Morgado, K. Raya, D. Binosi, L. Chang, J. Papavassiliou, C. D. Roberts, J. Rodríguez-Quintero, and S. M. Schmidt, Concerning pion parton distributions, Eur. Phys. J. A **58**, 10 (2022).
[28] Z. Zhu, Z. Hu, J. Lan, C. Mondal, X. Zhao, and J. P. Vary (BLFQ Collaboration), Transverse structure of the pion beyond leading twist with basis light-front quantization, Phys. Lett. B **839**, 137808 (2023).
[29] X. Gao, A. D. Hanlon, N. Karthik, S. Mukherjee, P. Petreczky, P. Scior, S. Shi, S. Syritsyn, Y. Zhao, and K. Zhou, Continuum-extrapolated NNLO valence PDF of the pion at the physical point, Phys. Rev. D **106**, 114510 (2022).
[30] N. Karthik, Quark distribution inside a pion in many-flavor $(2+1)$-dimensional QCD using lattice computations: UV listens to IR, Phys. Rev. D **103**, 074512 (2021).
[31] H.-W. Lin, J.-W. Chen, Z. Fan, J.-H. Zhang, and R. Zhang, Valence-quark distribution of the kaon and pion from lattice QCD, Phys. Rev. D **103**, 014516 (2021).
[32] X. Gao, L. Jin, C. Kallidonis, N. Karthik, S. Mukherjee, P. Petreczky, C. Shugert, S. Syritsyn, and Y. Zhao, Valence parton distribution of the pion from lattice QCD: Approaching the continuum limit, Phys. Rev. D **102**, 094513 (2020).
[33] R. S. Sufian, C. Egerer, J. Karpie, R. G. Edwards, B. Joó, Y.-Q. Ma, K. Orginos, J.-W. Qiu, and D. G. Richards, Pion valence quark distribution from current-current correlation in lattice QCD, Phys. Rev. D **102**, 054508 (2020).
[34] R. S. Sufian, J. Karpie, C. Egerer, K. Orginos, J.-W. Qiu, and D. G. Richards, Pion valence quark distribution from matrix element calculated in lattice QCD, Phys. Rev. D **99**, 074507 (2019).
[35] T. Izubuchi, L. Jin, C. Kallidonis, N. Karthik, S. Mukherjee, P. Petreczky, C. Shugert, and S. Syritsyn, Valence parton distribution function of pion from fine lattice, Phys. Rev. D **100**, 034516 (2019).
[36] B. Joó, J. Karpie, K. Orginos, A. V. Radyushkin, D. G. Richards, R. S. Sufian, and S. Zafeiropoulos, Pion valence structure from Ioffe-time parton pseudodistribution functions, Phys. Rev. D **100**, 114512 (2019).
[37] J.-H. Zhang, J.-W. Chen, L. Jin, H.-W. Lin, A. Schäfer, and Y. Zhao, First direct lattice-QCD calculation of the

x-dependence of the pion parton distribution function, Phys. Rev. D **100**, 034505 (2019).
[38] Z. Fan and H.-W. Lin, Gluon parton distribution of the pion from lattice QCD, Phys. Lett. B **823**, 136778 (2021).
[39] J. F. Owens, Q^2 dependent parametrizations of pion parton distribution functions, Phys. Rev. D **30**, 943 (1984).
[40] P. Aurenche, R. Baier, M. Fontannaz, M. N. Kienzle-Focacci, and M. Werlen, The gluon content of the pion from high p_T direct photon production, Phys. Lett. B **233**, 517 (1989).
[41] P. J. Sutton, A. D. Martin, R. G. Roberts, and W. J. Stirling, Parton distributions for the pion extracted from Drell-Yan and prompt photon experiments, Phys. Rev. D **45**, 2349 (1992).
[42] M. Gluck, E. Reya, and A. Vogt, Pionic parton distributions, Z. Phys. C **53**, 651 (1992).
[43] M. Gluck, E. Reya, and I. Schienbein, Pionic parton distributions revisited, Eur. Phys. J. C **10**, 313 (1999).
[44] C. Bourrely, W.-C. Chang, and J.-C. Peng, Pion partonic distributions in the statistical model from pion-induced Drell-Yan and J/Ψ production data, Phys. Rev. D **105**, 076018 (2022).
[45] C. Bourrely, F. Buccella, and J.-C. Peng, A new extraction of pion parton distributions in the statistical model, Phys. Lett. B **813**, 136021 (2021).
[46] C. Bourrely and J. Soffer, Statistical approach of pion parton distributions from Drell–Yan process, Nucl. Phys. **A981**, 118 (2019).
[47] W.-C. Chang, J.-C. Peng, S. Platchkov, and T. Sawada, Constraining gluon density of pions at large x by pion-induced J/ψ production, Phys. Rev. D **102**, 054024 (2020).
[48] P. C. Barry, N. Sato, W. Melnitchouk, and C.-R. Ji, First Monte Carlo Global QCD Analysis of Pion Parton Distributions, Phys. Rev. Lett. **121**, 152001 (2018).
[49] P. C. Barry, C.-R. Ji, N. Sato, and W. Melnitchouk (Jefferson Lab Angular Momentum (JAM) Collaboration), Global QCD Analysis of Pion Parton Distributions with Threshold Resummation, Phys. Rev. Lett. **127**, 232001 (2021).
[50] P. C. Barry *et al.* (Jefferson Lab Angular Momentum (JAM) and HadStruc Collaborations), Complementarity of experimental and lattice QCD data on pion parton distributions, Phys. Rev. D **105**, 114051 (2022).
[51] J. Arrington *et al.*, Physics with CEBAF at 12 GeV and future opportunities, Prog. Part. Nucl. Phys. **127**, 103985 (2022).
[52] R. Abdul Khalek *et al.*, Science requirements and detector concepts for the electron-ion collider: EIC yellow report, Nucl. Phys. **A1026**, 122447 (2022).
[53] D. P. Anderle *et al.*, Electron-ion collider in China, Front. Phys. **16**, 64701 (2021).
[54] J. D. Sullivan, One pion exchange and deep inelastic electron—nucleon scattering, Phys. Rev. D **5**, 1732 (1972).
[55] A. C. Aguilar *et al.*, Pion and kaon structure at the electron-ion collider, Eur. Phys. J. A **55**, 190 (2019).
[56] J. Arrington *et al.*, Revealing the structure of light pseudoscalar mesons at the electron–ion collider, J. Phys. G **48**, 075106 (2021).
[57] B. Adams *et al.*, Letter of intent: A new QCD facility at the M2 beam line of the CERN SPS (COMPASS++/AMBER), arXiv:1808.00848.
[58] G. P. Lepage and S. J. Brodsky, Exclusive processes in quantum chromodynamics: Evolution equations for hadronic wave functions and the form-factors of mesons, Phys. Lett. **87B**, 359 (1979).
[59] A. V. Efremov and A. V. Radyushkin, Factorization and asymptotical behavior of pion form-factor in QCD, Phys. Lett. **94B**, 245 (1980).
[60] J. P. B. C. de Melo, T. Frederico, E. Pace, and G. Salmè, Electromagnetic form-factor of the pion in the space and time-like regions within the front form dynamics, Phys. Lett. B **581**, 75 (2004).
[61] J. P. B. C. de Melo, T. Frederico, E. Pace, and G. Salmè, Pair term in the electromagnetic current within the front form dynamics: Spin-0 case, Nucl. Phys. **A707**, 399 (2002).
[62] C.-W. Hwang, A Consistent treatment for pion form-factors in spacelike and timelike regions, Phys. Rev. D **64**, 034011 (2001).
[63] B. L. G. Bakker, H.-M. Choi, and C.-R. Ji, Regularizing the fermion loop divergencies in the light front meson currents, Phys. Rev. D **63**, 074014 (2001).
[64] F. Cardarelli, I. L. Grach, I. M. Narodetsky, E. Pace, G. Salmè, and S. Simula, Charge form-factor of pi and K mesons, Phys. Rev. D **53**, 6682 (1996).
[65] F. Cardarelli, E. Pace, G. Salmè, and S. Simula, Nucleon and pion electromagnetic form-factors in a light front constituent quark model, Phys. Lett. B **357**, 267 (1995).
[66] T. Frederico and G. A. Miller, Null plane phenomenology for the pion decay constant and radius, Phys. Rev. D **45**, 4207 (1992).
[67] P. L. Chung, F. Coester, and W. N. Polyzou, Charge form-factors of quark model pions, Phys. Lett. B **205**, 545 (1988).
[68] X. Gao, N. Karthik, S. Mukherjee, P. Petreczky, S. Syritsyn, and Y. Zhao, Pion form factor and charge radius from lattice QCD at the physical point, Phys. Rev. D **104**, 114515 (2021).
[69] C. Alexandrou, S. Bacchio, I. Cloet, M. Constantinou, J. Delmar, K. Hadjiyiannakou, G. Koutsou, C. Lauer, and A. Vaquero (ETM Collaboration), Scalar, vector, and tensor form factors for the pion and kaon from lattice QCD, Phys. Rev. D **105**, 054502 (2022).
[70] G. Wang, J. Liang, T. Draper, K.-F. Liu, and Y.-B. Yang (chiQCD Collaboration), Lattice calculation of pion form factor with overlap fermions, Phys. Rev. D **104**, 074502 (2021).
[71] C. Alexandrou *et al.* (ETM Collaboration), Pion vector form factor from lattice QCD at the physical point, Phys. Rev. D **97**, 014508 (2018).
[72] S. Aoki, G. Cossu, X. Feng, S. Hashimoto, T. Kaneko, J. Noaki, and T. Onogi (JLQCD Collaboration), Light meson electromagnetic form factors from three-flavor lattice QCD with exact chiral symmetry, Phys. Rev. D **93**, 034504 (2016).
[73] J. Koponen, F. Bursa, C. T. H. Davies, R. J. Dowdall, and G. P. Lepage, Size of the pion from full lattice QCD with

physical u, d, s and c quarks, Phys. Rev. D **93**, 054503 (2016).
[74] H. Fukaya, S. Aoki, S. Hashimoto, T. Kaneko, H. Matsufuru, and J. Noaki, Computation of the electromagnetic pion form factor from lattice QCD in the ϵ regime, Phys. Rev. D **90**, 034506 (2014).
[75] B. B. Brandt, A. Jüttner, and H. Wittig, The pion vector form factor from lattice QCD and NNLO chiral perturbation theory, J. High Energy Phys. 11 (2013) 034.
[76] O. H. Nguyen, K.-I. Ishikawa, A. Ukawa, and N. Ukita, Electromagnetic form factor of pion from $N_f = 2 + 1$ dynamical flavor QCD, J. High Energy Phys. 04 (2011) 122.
[77] S. Aoki *et al.* (JLQCD and TWQCD Collaborations), Pion form factors from two-flavor lattice QCD with exact chiral symmetry, Phys. Rev. D **80**, 034508 (2009).
[78] R. Frezzotti, V. Lubicz, and S. Simula (ETM Collaboration), Electromagnetic form factor of the pion from twisted-mass lattice QCD at $N(f) = 2$, Phys. Rev. D **79**, 074506 (2009).
[79] P. A. Boyle, J. M. Flynn, A. Juttner, C. Kelly, H. P. de Lima, C. M. Maynard, C. T. Sachrajda, and J. M. Zanotti, The Pion's electromagnetic form-factor at small momentum transfer in full lattice QCD, J. High Energy Phys. 07 (2008) 112.
[80] D. Brömmel *et al.* (QCDSF/UKQCD Collaboration), The Pion form-factor from lattice QCD with two dynamical flavours, Eur. Phys. J. C **51**, 335 (2007).
[81] F. D. R. Bonnet, R. G. Edwards, G. T. Fleming, R. Lewis, and D. G. Richards (Lattice Hadron Physics Collaboration), Lattice computations of the pion form-factor, Phys. Rev. D **72**, 054506 (2005).
[82] X. Feng, Y. Fu, and L.-C. Jin, Lattice QCD calculation of the pion charge radius using a model-independent method, Phys. Rev. D **101**, 051502 (2020).
[83] E. B. Dally *et al.*, Measurement of the π^- form-factor, Phys. Rev. D **24**, 1718 (1981).
[84] E. B. Dally *et al.*, Elastic Scattering Measurement of the Negative Pion Radius, Phys. Rev. Lett. **48**, 375 (1982).
[85] S. R. Amendolia *et al.*, A measurement of the pion charge radius, Phys. Lett. **146B**, 116 (1984).
[86] S. R. Amendolia *et al.* (NA7 Collaboration), A measurement of the space-like pion electromagnetic form-factor, Nucl. Phys. **B277**, 168 (1986).
[87] C. J. Bebek, C. N. Brown, M. Herzlinger, S. D. Holmes, C. A. Lichtenstein, F. M. Pipkin, S. Raither, and L. K. Sisterson, Measurement of the pion form-factor up to $q^2 = 4$ GeV^2, Phys. Rev. D **13**, 25 (1976).
[88] C. J. Bebek *et al.*, Scalar Transverse Separation for Single π^+ Electroproduction, Phys. Rev. Lett. **37**, 1326 (1976).
[89] C. J. Bebek *et al.*, Electroproduction of single pions at low epsilon and a measurement of the pion form-factor up to $q^2 = 10$ GeV^2, Phys. Rev. D **17**, 1693 (1978).
[90] P. Brauel, T. Canzler, D. Cords, R. Felst, G. Grindhammer, M. Helm, W. D. Kollmann, H. Krehbiel, and M. Schadlich, Electroproduction of $\pi^+ n$, $\pi^- p$ and $K^+\Lambda$, $K^+\Sigma^0$ final states above the resonance region, Z. Phys. C **3**, 101 (1979).
[91] H. Ackermann, T. Azemoon, W. Gabriel, H. D. Mertiens, H. D. Reich, G. Specht, F. Janata, and D. Schmidt, Determination of the longitudinal and the transverse part in pi + electroproduction, Nucl. Phys. **B137**, 294 (1978).
[92] J. Volmer *et al.* (Jefferson Lab F(pi) Collaboration), Measurement of the Charged Pion Electromagnetic Form-Factor, Phys. Rev. Lett. **86**, 1713 (2001).
[93] V. Tadevosyan *et al.* (Jefferson Lab F(pi) Collaboration), Determination of the pion charge form-factor for $Q^2 = 0.60$ GeV^2—1.60 GeV^2, Phys. Rev. C **75**, 055205 (2007).
[94] T. Horn *et al.* (Jefferson Lab F(pi) Collaboration), Determination of the Charged Pion Form Factor at $Q^2 = 1.60$ and 2.45-$(\mathrm{GeV}/c)^2$, Phys. Rev. Lett. **97**, 192001 (2006).
[95] H. P. Blok *et al.* (Jefferson Lab Collaboration), Charged pion form factor between $Q^2 = 0.60$ and 2.45 GeV^2. I. Measurements of the cross section for the $^1\mathrm{H}(e, e'\pi^+)n$ reaction, Phys. Rev. C **78**, 045202 (2008).
[96] G. M. Huber *et al.* (Jefferson Lab Collaboration), Charged pion form-factor between $Q^2 = 0.60$ GeV^2 and 2.45 GeV^2. II. Determination of, and results for, the pion form-factor, Phys. Rev. C **78**, 045203 (2008).
[97] S. Alekhin *et al.*, HERAFitter, Eur. Phys. J. C **75**, 304 (2015).
[98] I. Novikov *et al.*, Parton distribution functions of the charged pion within the xFitter framework, Phys. Rev. D **102**, 014040 (2020).
[99] A. V. Radyushkin, Deep elastic processes of composite particles in field theory and asymptotic freedom, arXiv: hep-ph/0410276.
[100] V. L. Chernyak and A. R. Zhitnitsky, Asymptotic behavior of hadron form-factors in quark model (in Russian), JETP Lett. **25**, 510 (1977).
[101] V. L. Chernyak and A. R. Zhitnitsky, Asymptotics of hadronic form-factors in the quantum chromodynamics (in Russian), Sov. J. Nucl. Phys. **31**, 544 (1980).
[102] V. L. Chernyak, A. R. Zhitnitsky, and V. G. Serbo, Asymptotic hadronic form-factors in quantum chromodynamics, JETP Lett. **26**, 594 (1977).
[103] V. L. Chernyak, V. G. Serbo, and A. R. Zhitnitsky, Calculation of asymptotics of the pion electromagnetic form-factor in the QCD perturbation theory (in Russian), Sov. J. Nucl. Phys. **31**, 552 (1980).
[104] S. J. Brodsky, T. Huang, and P. Lepage, in *Particle and Fields*, edited by A. Z. Capri and A. N. Kamal (Plenum, New York, 1983).
[105] V. M. Braun and I. E. Filyanov, Conformal invariance and pion wave functions of nonleading twist, Z. Phys. C **48**, 239 (1990).
[106] B. Betev *et al.* (NA10 Collaboration), Differential cross-section of high mass muon pairs produced by a 194-GeV/$c\pi^-$ beam on a tungsten target, Z. Phys. C **28**, 9 (1985).
[107] J. S. Conway *et al.*, Experimental study of muon pairs produced by 252-GeV pions on tungsten, Phys. Rev. D **39**, 92 (1989).
[108] M. Bonesini *et al.* (WA70 Collaboration), High transverse momentum prompt photon production by π^- and π^+ on protons at 280-GeV/c, Z. Phys. C **37**, 535 (1988).
[109] F. James and M. Roos, MINUIT: A system for function minimization and analysis of the parameter errors and correlations, Comput. Phys. Commun. **10**, 343 (1975).

[110] M. Aicher, A. Schäfer, and W. Vogelsang, Soft-Gluon Resummation and the Valence Parton Distribution Function of the Pion, Phys. Rev. Lett. **105**, 252003 (2010).
[111] M. Ding, K. Raya, D. Binosi, L. Chang, C. D. Roberts, and S. M. Schmidt, Symmetry, symmetry breaking, and pion parton distributions, Phys. Rev. D **101**, 054014 (2020).
[112] Z.-F. Cui, M. Ding, F. Gao, K. Raya, D. Binosi, L. Chang, C. D. Roberts, J. Rodríguez-Quintero, and S. M. Schmidt, Kaon and pion parton distributions, Eur. Phys. J. C **80**, 1064 (2020).
[113] H. B. Meyer and J. W. Negele, Gluon contributions to the pion mass and light cone momentum fraction, Phys. Rev. D **77**, 037501 (2008).
[114] P. E. Shanahan and W. Detmold, Gluon gravitational form factors of the nucleon and the pion from lattice QCD, Phys. Rev. D **99**, 014511 (2019).
[115] M. Oehm, C. Alexandrou, M. Constantinou, K. Jansen, G. Koutsou, B. Kostrzewa, F. Steffens, C. Urbach, and S. Zafeiropoulos, $\langle x \rangle$ and $\langle x^2 \rangle$ of the pion PDF from lattice QCD with $N_f = 2 + 1 + 1$ dynamical quark flavors, Phys. Rev. D **99**, 014508 (2019).
[116] C. Alexandrou *et al.* (Extended Twisted Mass Collaboration), Quark and Gluon Momentum Fractions in the Pion from $Nf = 2 + 1 + 1$ Lattice QCD, Phys. Rev. Lett. **127**, 252001 (2021).
[117] J. D. Sullivan, On the importance of pion electroproduction at high energy, Phys. Lett. **33B**, 179 (1970).
[118] P. Pedroni and S. Sconfietti, A new Monte Carlo-based fitting method, J. Phys. G **47**, 054001 (2020).
[119] P. C. Barry, L. Gamberg, W. Melnitchouk, E. Moffat, D. Pitonyak, A. Prokudin, and N. Sato, Tomography of pions and protons via transverse momentum dependent distributions, arXiv:2302.01192.
[120] A. Vladimirov, Pion-induced Drell-Yan processes within TMD factorization, J. High Energy Phys. 10 (2019) 090.
[121] M. Cerutti, L. Rossi, S. Venturini, A. Bacchetta, V. Bertone, C. Bissolotti, and M. Radici (MAP Collaboration), Extraction of pion transverse momentum distributions from Drell-Yan data, Phys. Rev. D **107**, 014014 (2023).